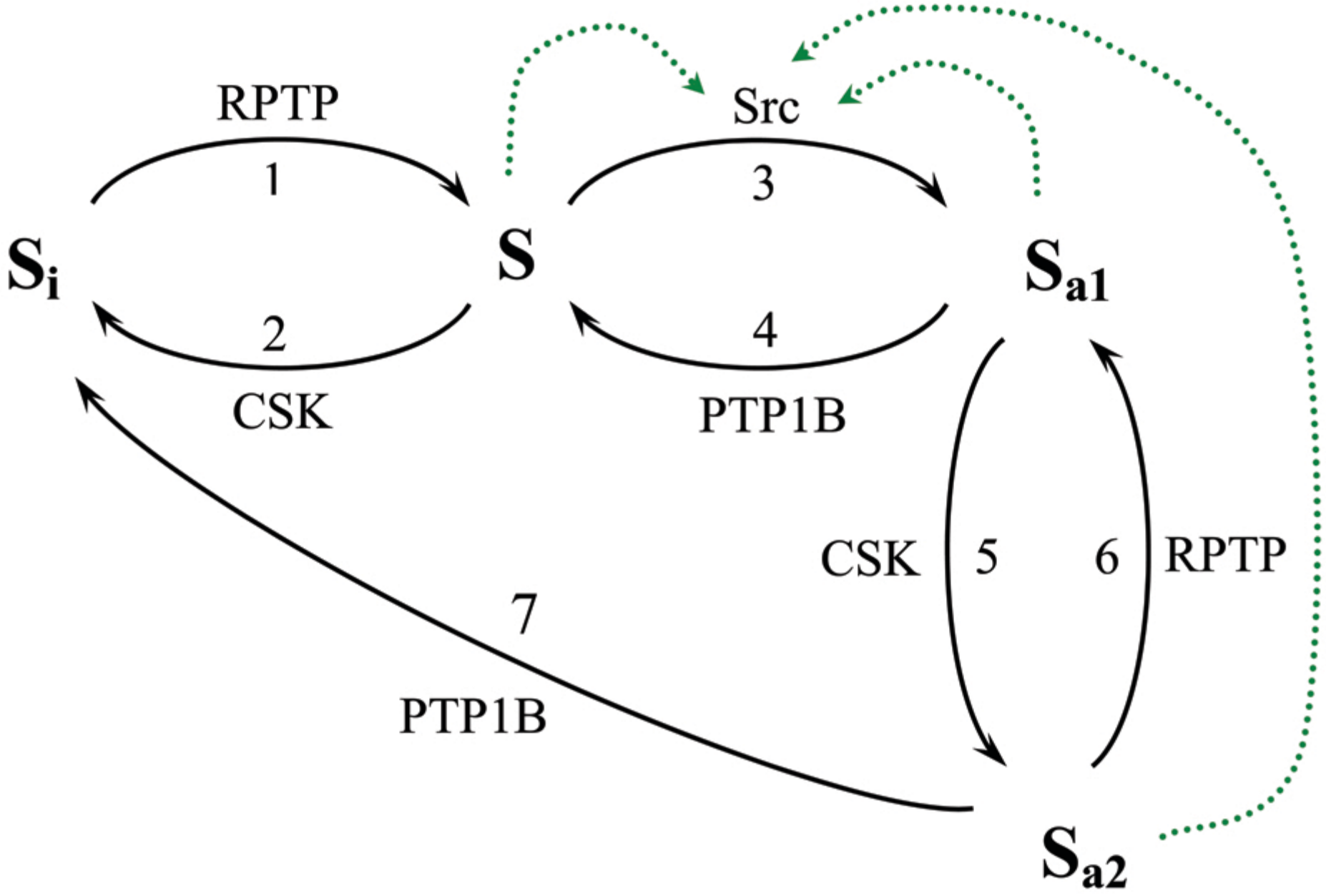

Fig. 1

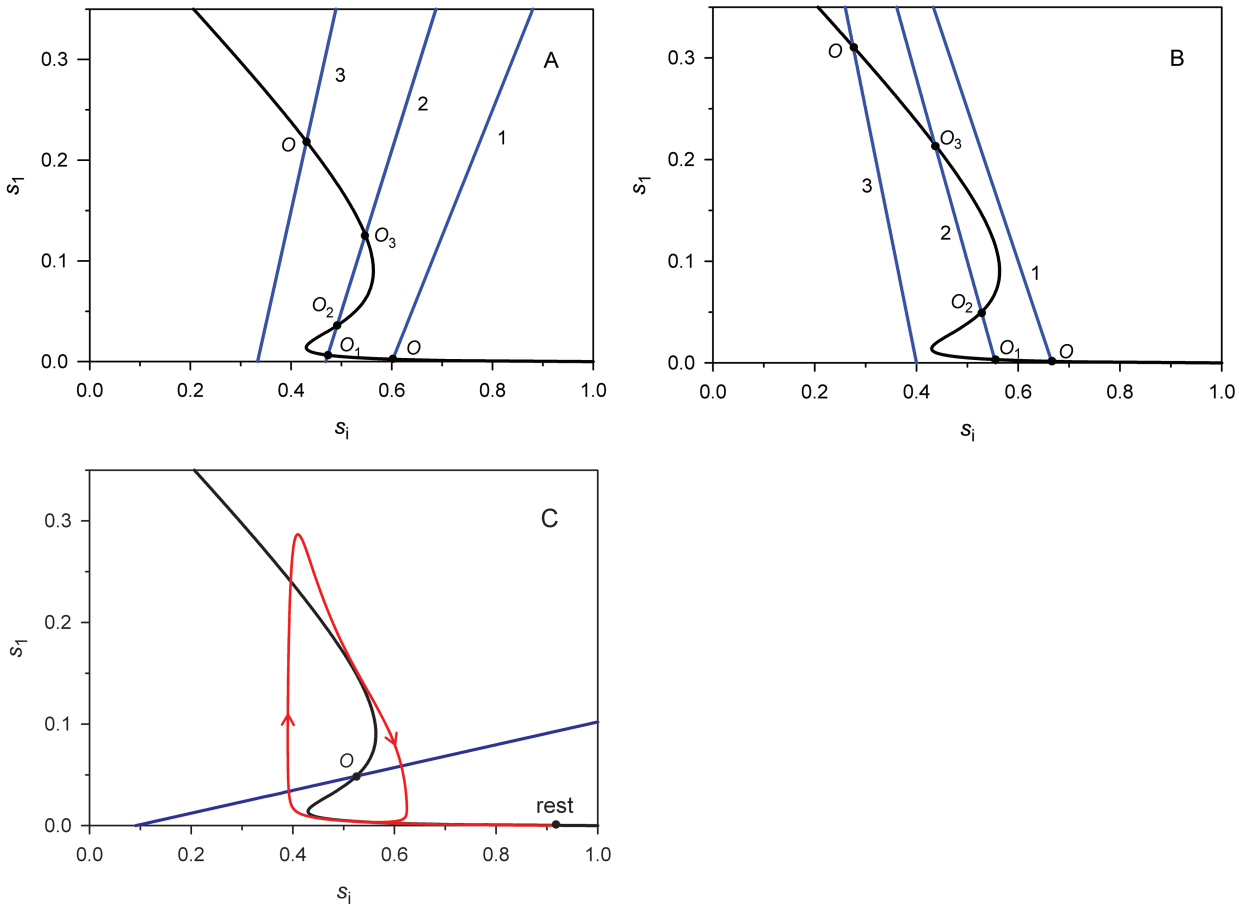

Fig. 2

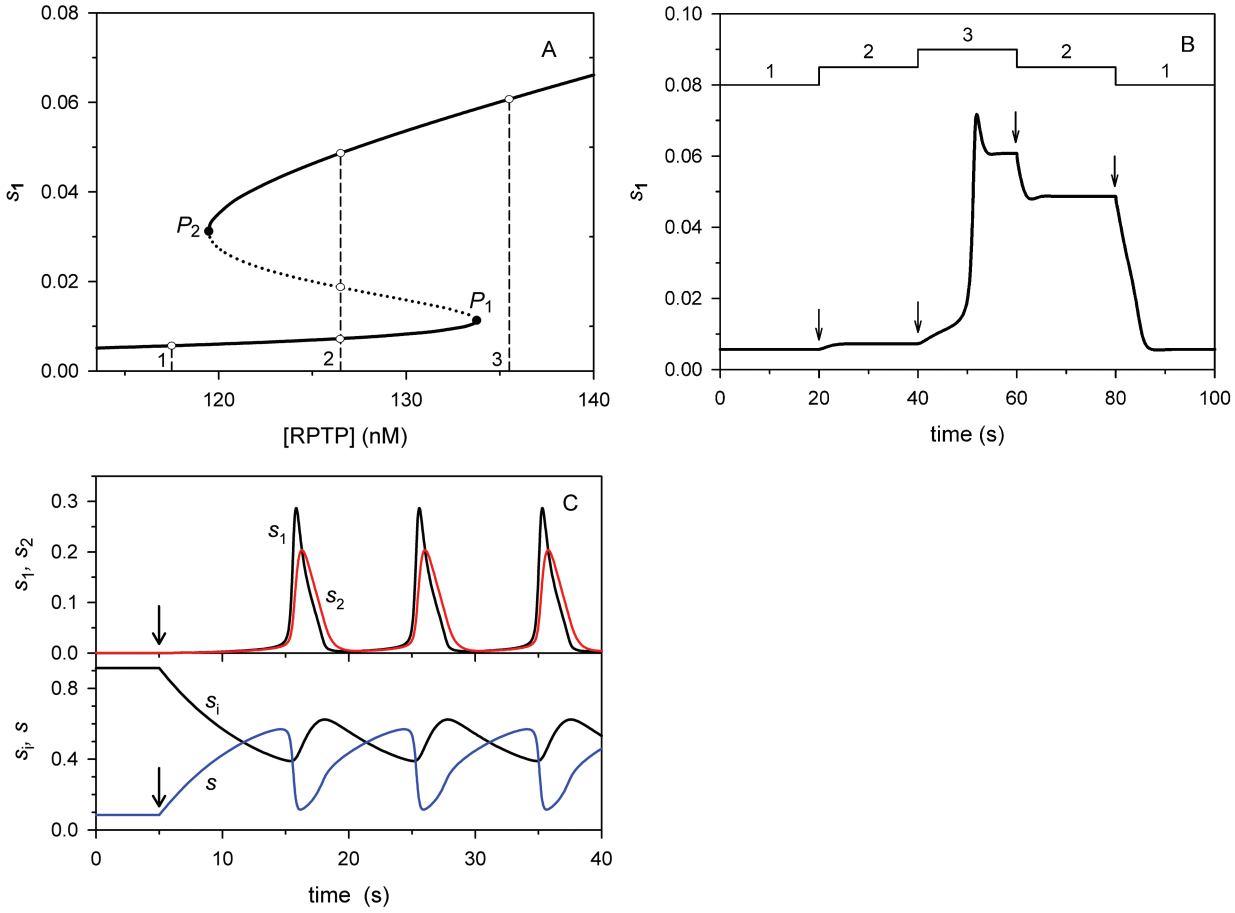

Fig. 3

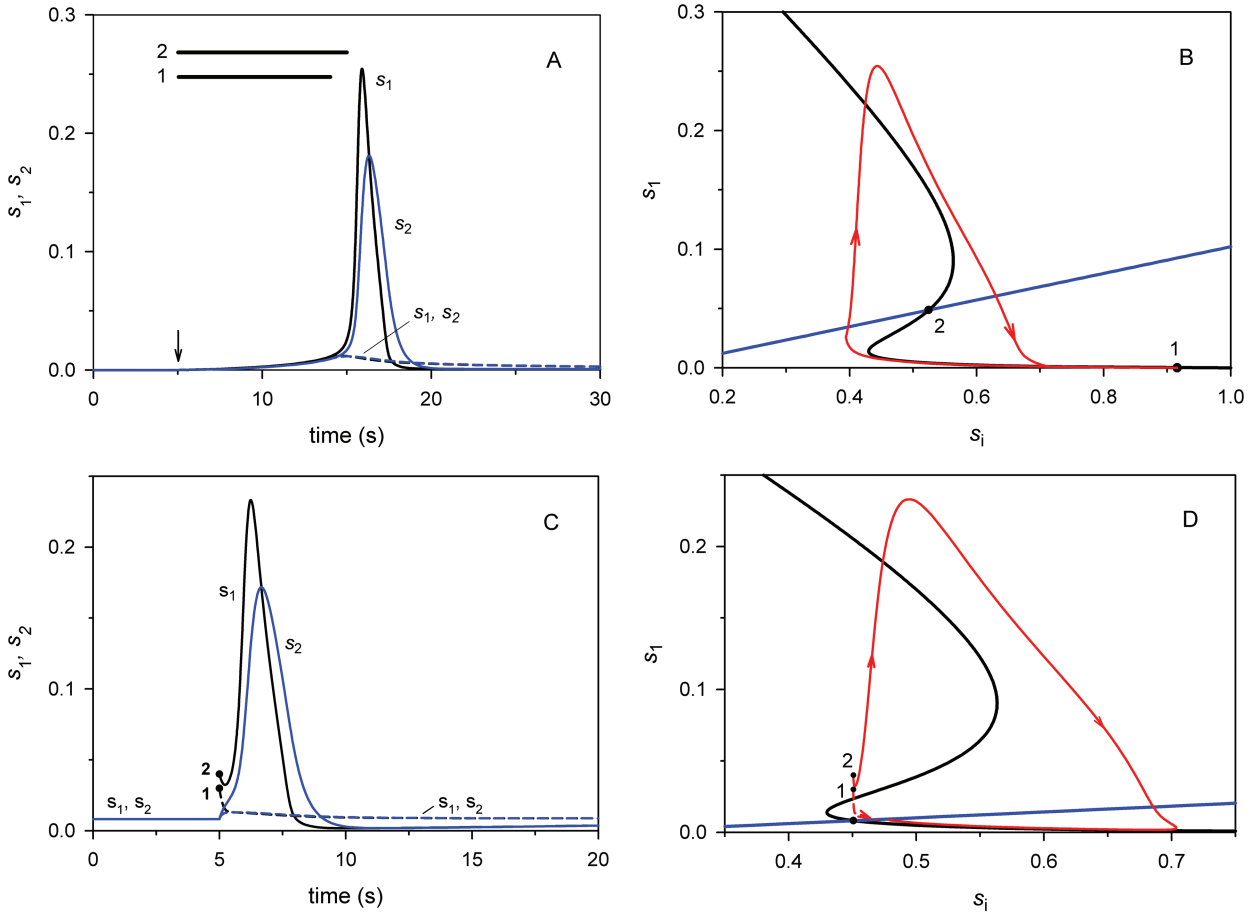
A
B
C
D
2
1
s_1
s_2
s_1, s_2
time (s)
s_i
s_1
0.0
0.1
0.2
0.3
0
10
20
30
0.2
0.4
0.6
0.8
1.0
5
15
0.4
0.5
0.6
0.7

Fig. 4

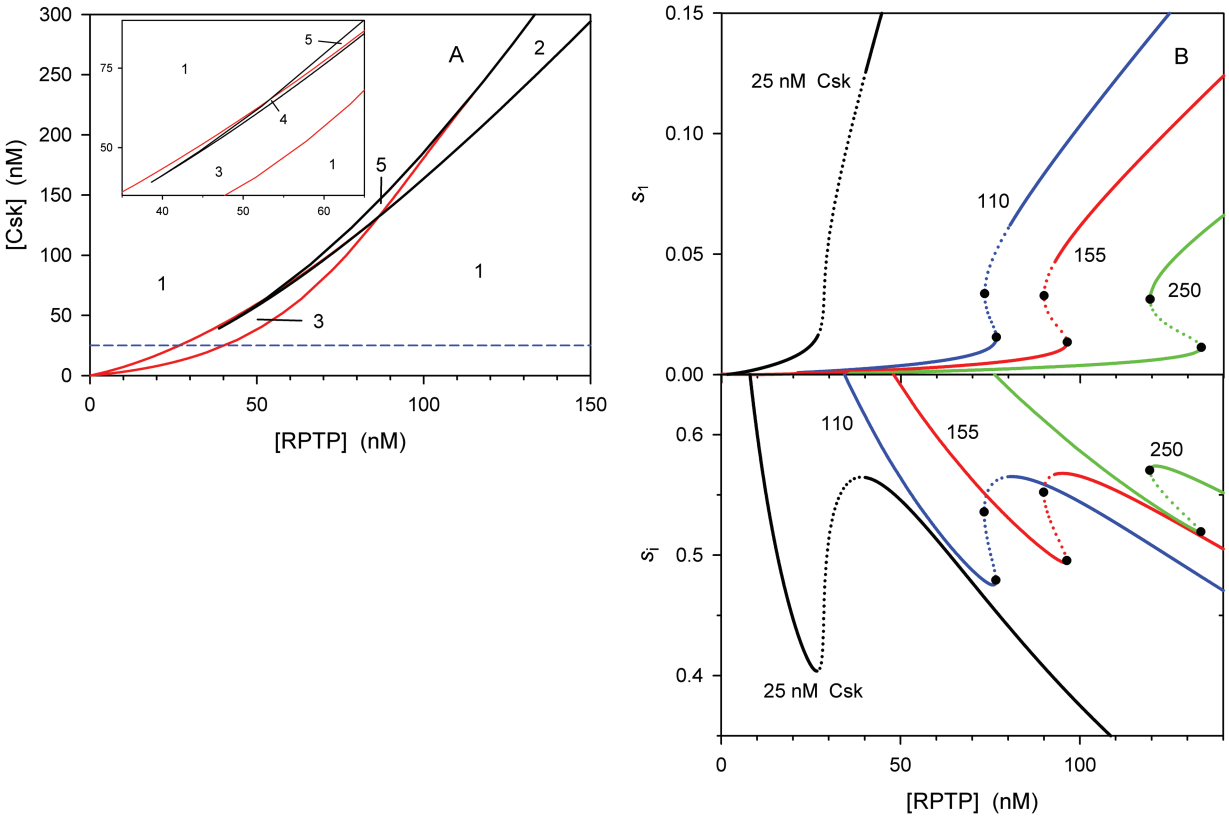

Fig. 5

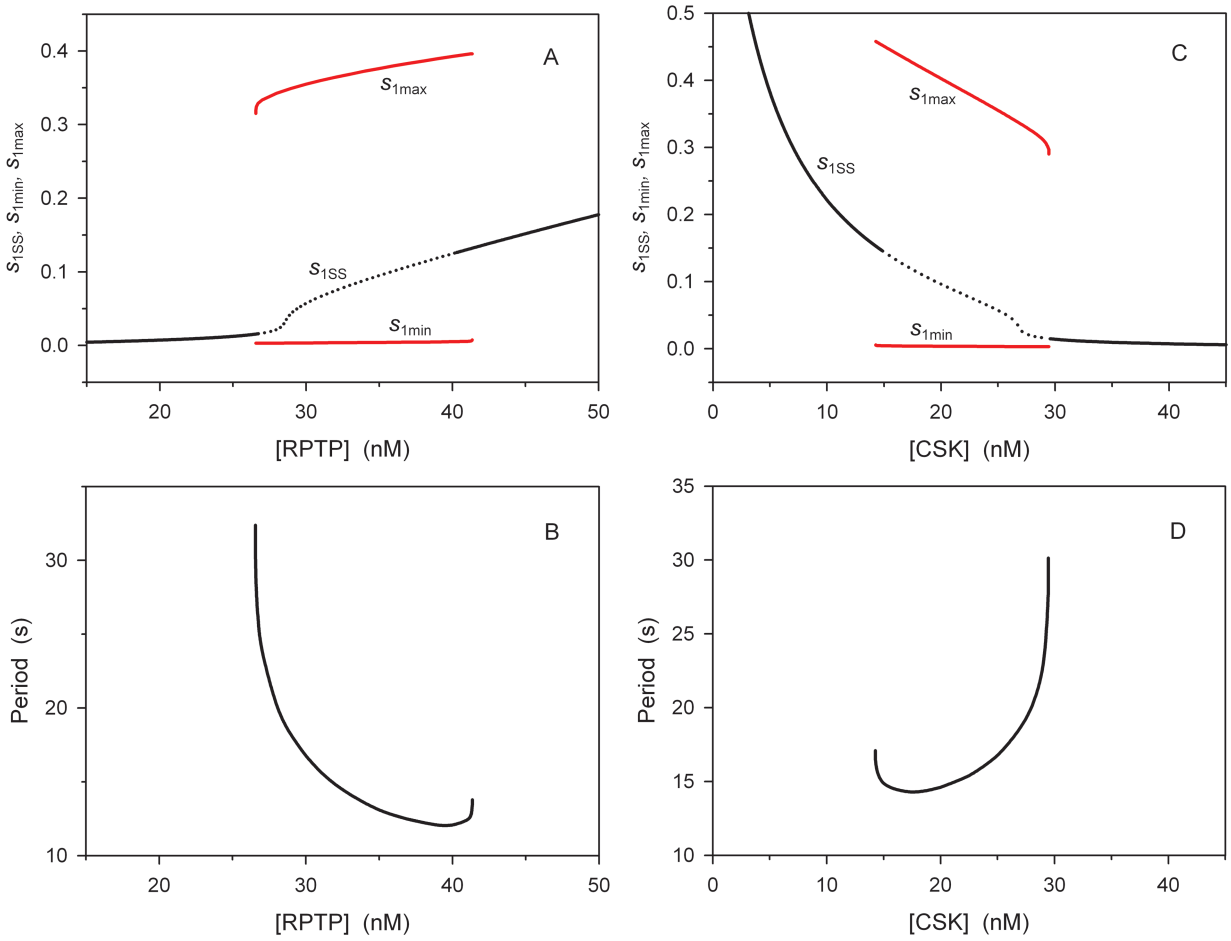
A
B
C
D
s_{1max}
s_{1SS}
s_{1min}
s_{1SS}, s_{1min}, s_{1max}
[RPTP] (nM)
[CSK] (nM)
Period (s)

Fig. 6

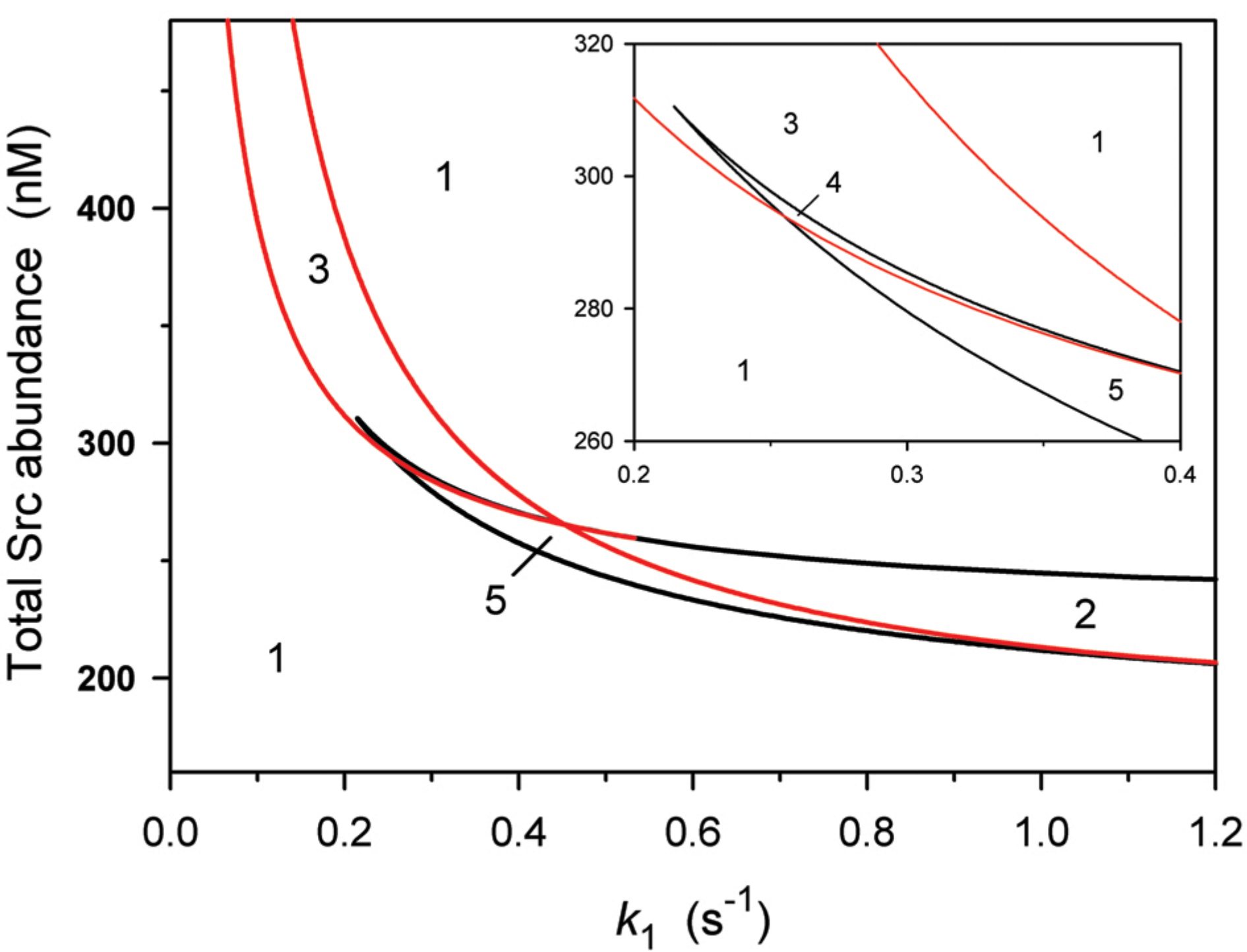
Total Src abundance (nM)
400
300
200
0.0
0.2
0.4
0.6
0.8
1.0
1.2
k_1 (s^{-1})
1
2
3
5
320
300
280
260
0.2
0.3
0.4
4

Fig. 7

Online supplementary material

Toggle switches, pulses and oscillations are intrinsic properties of the Src activation/deactivation cycle.

Nikolai P. Kaimachnikov[1,2] and Boris N. Kholodenko[1,3*]

[1] Department of Pathology, Anatomy and Cell Biology, Thomas Jefferson University, Philadelphia, PA, USA

[2] Institute of Cell Biophysics, Russian Academy of Science, Pushchino, Moscow region, Russia.

[3]Systems Biology Ireland, University College Dublin, Belfield, Dublin, Ireland

[*]**Corresponding author**
Boris N. Kholodenko
E-mail: Boris.Kholodenko@ucd.ie

Content

Table S1 contains ranges of kinetic parameters and references.
Fig. S1 shows graphical and analytical solutions to the quasi steady-state (QSS) equations of the kinetic model.
Fig. S2 illustrates that the proximity of the Src initial state to the excitability threshold decreases the lag period.
Fig. S3 presents a complete numerical investigation of the dependence of the Z-shaped QSS curve on each kinetic parameter involved.
Fig. S4 shows the effects of reaction rate saturability on the QSS dependencies.
Fig. S5 demonstrates how the Z-shaped QSS curve changes with the increase in the concentrations of Src dimers.

Table S1. Range of kinetic parameters.

The first-order rate constants, k_1, k_2, k_5, k_6 and k_7, approximate the $k^{cat}[\mathrm{E}]/K_M = V^{\max}/K_M$ ratios for the corresponding enzyme reactions. Protein abundances are assumed to be in a typical range for intracellular signaling proteins, 10-1000 nM.

Parameter, Enzyme	K_M (nM)	k^{cat} (s^{-1})	Parameter range (s^{-1})	Values exploited in numerical analysis
k_1, k_6 PTPα	$(1.8–3.7)\cdot10^5$ [1][a]	13–34 [1][a]	$4.8\cdot10^{-4}$–0.19	k_1=0.001–1.5 (Figs. 2-6) k_6=1 (Figs. 2-4, 6, S1-S4[c]) $0 < k_6 < 3$ (Fig. 5)
	$1.5\cdot10^4$ [2]	1.7 [2]	0.0011–0.11	
k_1, k_6 PTPε	$3.7\cdot10^4$ [2]	20 [2]	0.0054–0.54	
k_2, k_5 Csk[d]	1270/210 [3][b]	1.8 [5]	0.014–1.4/ 0.086–8.6	k_2=0.01–1 (Figs. 2-4, 6, S2, S4[c]) $0 < k_2 < 0.6$ (Fig. 5) k_5=2 (Figs. 2-4, 6, S2, S4 C-F) $0 < k_5 < 12$ (Fig. 5) k_5=20 (Fig. S4[c] A,B)
	3500 [4]	1.3 [4]	0.004–0.4	
	5400 [5]	1.8 [5]	0.003–0.3	
	6200/2800 [6][b]	0.14/0.12 [6][b]	0.0002–0.02/ 0.0004–0.04	
$k_4 = V_4^{\max}/S^{tot}$ PTP1B	N/A	26 [7, 8]	0.26–260[e]	k_4=1 (Figs. 2-6, S1–S4) k_4=0.2, 1, 2 (Fig. S3B)
		67 [9]	0.67–670[e]	
$\beta = K_4/S^{tot}$ PTP1B	110-280 [7, 8][a]	N/A	0.1-1[f] (dimensionless)	0.01 (Figs. 2-6, S1–S4) 0.001, 0.01, 0.1 (Fig. S3C)
k_7 PTP1B		26 [7, 8]	0.9–24	k_7=1 (Figs. 2-6, S1-S4) k_7=0, 1, 10 (Fig. S3F)
		67 [9]	2.4–61	

[a]Data obtained with different peptide substrates.

[b]Data obtained in the absence or presence of Cbp.

[c]In Fig. S4, the Michaelis-Menten rate laws are considered. Accordingly, new parameters and their ranges are introduced, see the legend to Fig. S4.

[d]As the experimental data show that autophosphorylation facilitates the phosphorylation of SFK by Csk [10, 11], we explore both equal and different rate constants (k_2, k_5) for two Src conformations (S and S_{a1}).

[e]PTP1B abundance was reported to be 10 – 100 nM [8, 12].

[f]Saturability of PTP1B in vivo was determined in live cells loaded with a synthetic phosphopeptide using Förster resonant energy transfer for imaging enzyme-substrate (ES) intermediates; K_M/[S] appeared to be in a range 0.1 – 1 in different cellular compartments [9].

References

1. Wu L, Buist A, den Hertog J & Zhang ZY (1997) Comparative kinetic analysis and substrate specificity of the tandem catalytic domains of the receptor-like protein-tyrosine phosphatase alpha. *J Biol Chem* **272**, 6994-7002.
2. Lim KL, Lai DS, Kalousek MB, Wang Y & Pallen CJ (1997) Kinetic analysis of two closely related receptor-like protein-tyrosine-phosphatases, PTP alpha and PTP epsilon. *Eur J Biochem* **245**, 693-700.
3. Takeuchi S, Takayama Y, Ogawa A, Tamura K & Okada M (2000) Transmembrane phosphoprotein Cbp positively regulates the activity of the carboxyl-terminal Src kinase, Csk. *J Biol Chem* **275**, 29183-29186.
4. Wang D, Huang XY & Cole PA (2001) Molecular determinants for Csk-catalyzed tyrosine phosphorylation of the Src tail. *Biochemistry* **40**, 2004-2010.

5. Sondhi D, Xu W, Songyang Z, Eck MJ & Cole PA (1998) Peptide and protein phosphorylation by protein tyrosine kinase Csk: insights into specificity and mechanism, *Biochemistry* **37**, 165-172.
6. Wong L, Lieser SA, Miyashita O, Miller M, Tasken K, Onuchic JN, Adams JA, Woods VL, Jr. & Jennings PA (2005) Coupled motions in the SH2 and kinase domains of Csk control Src phosphorylation. *J Mol Biol* **351**, 131-143.
7. Tonks NK, Diltz CD & Fischer EH (1988) Characterization of the major protein-tyrosine-phosphatases of human placenta. *J Biol Chem* **263**, 6731-6737.
8. Zhang ZY (1997) Structure, mechanism, and specificity of protein-tyrosine phosphatases. *Curr Top Cell Regul* **35**, 21-68.
9. Yudushkin IA, Schleifenbaum A, Kinkhabwala A, Neel BG, Schultz C & Bastiaens PI (2007) Live-cell imaging of enzyme-substrate interaction reveals spatial regulation of PTP1B. *Science* **315**, 115-119.
10. Bougeret C, Delaunay T, Romero F, Jullien P, Sabe H, Hanafusa H, Benarous R & Fischer S (1996) Detection of a physical and functional interaction between Csk and Lck which involves the SH2 domain of Csk and is mediated by autophosphorylation of Lck on tyrosine 394. *J Biol Chem* **271**, 7465-7472.
11. Amrein KE, Molnos J, zur Hausen JD, Flint N, Takacs B & Burn P (1998) Csk-mediated phosphorylation of substrates is regulated by substrate tyrosine phosphorylation. *Farmaco* **53**, 266-272.
12. Tonks NK, Diltz CD & Fischer EH (1988) Purification of the major protein-tyrosine-phosphatases of human placenta. *J Biol Chem* **263**, 6722-6730.

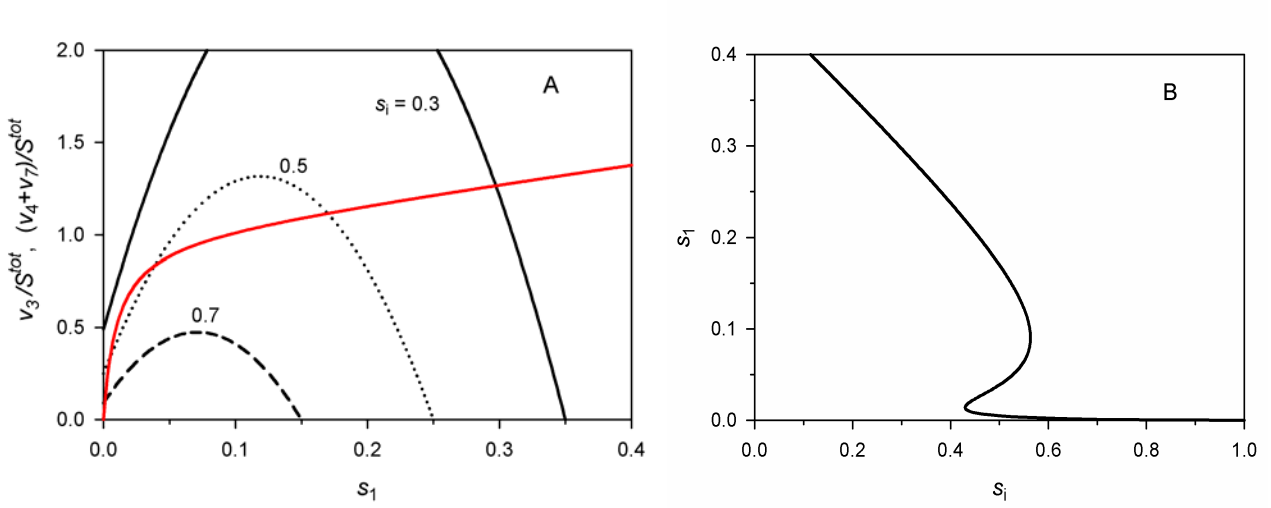

Fig. S1. Graphical and analytical solutions of the QSS equations for the kinetic model. The QSS curve that satisfies Eq. 10 of the main text is found by equating the time derivatives in Eqs. 7 and 8 to zero, resulting in the equation, $v_3 = v_4 + v_7$. **A**. Graphical analysis: plots present a family of the v_3 dependencies on s_1 at different s_i (indicated at each curve) and the function $v_4 + v_7$ (red) that depends only on s_1 (at QSS conditions where Eq. 9 applies). Points of intersections determine the QSS relationship between variables s_1 and s_i. At low and high s_i there is a single intersection point, whereas at the intermediate s_i three intersection points appear and, therefore, three different s_1 values correspond to a single s_i value. **B**. The QSS curve is plotted using the analytical solution to Eq. 10, $s_i = \left(f_1 - \sqrt{f_1^2 - 4\delta\, f_2}\right)/2\delta$, where $f_1 = 2\delta + (1-2\delta)(1+\xi)s_1$, $f_2 = (1-(1+\xi)s_1)\left(\delta + (1-\delta)(1+\xi)s_1\right) - (k_4 s_1/(\beta + s_1) + k_7 \xi s_1)/S^{tot}k_3$. Parameter values are k_3=20, k_4=1, k_7=1 (s^{-1}), β=0.01, δ=0.05, $\xi = 1$.

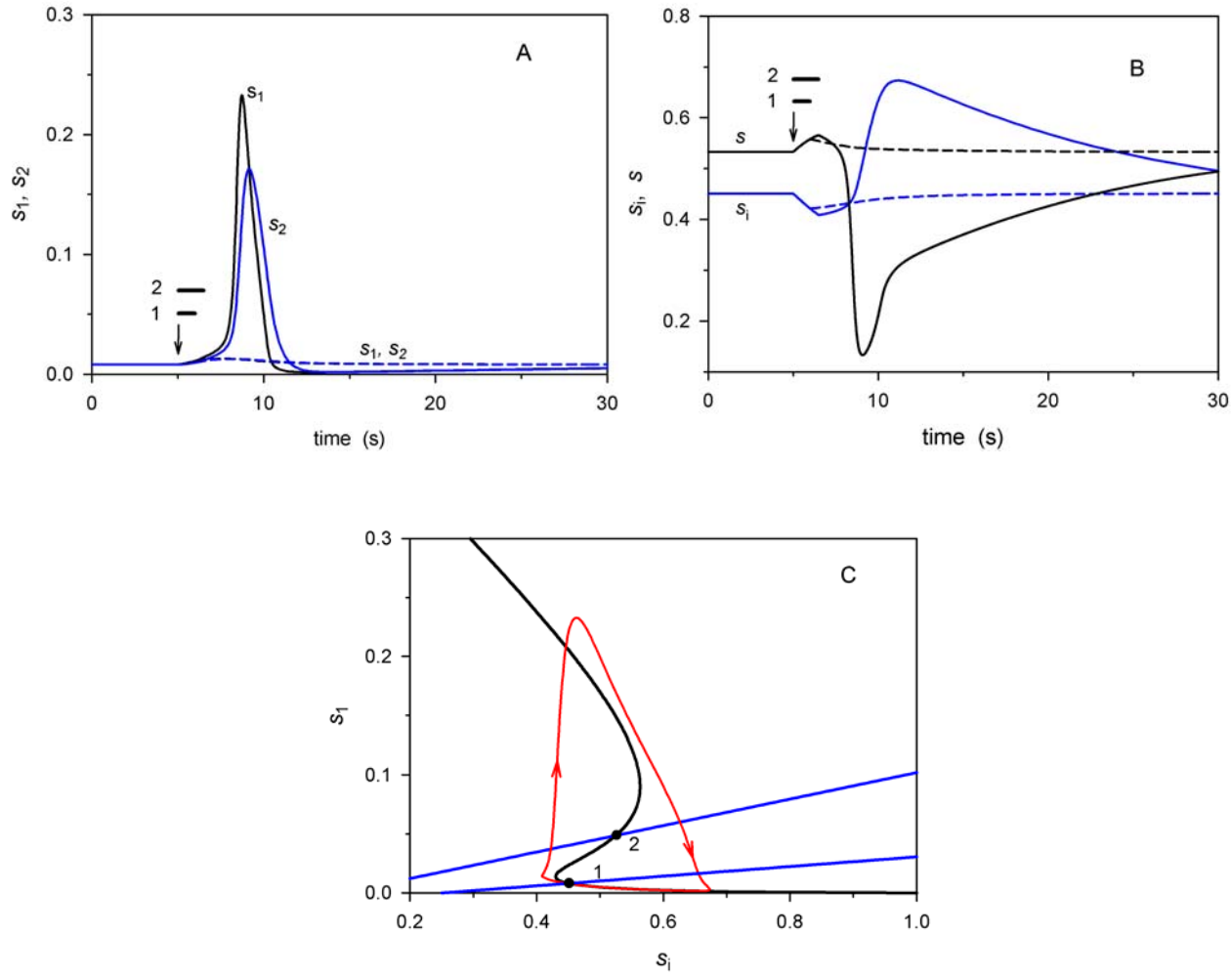

Fig. S2. Proximity of Src initial state to the excitability threshold decreases the lag period. Time-dependent responses to sub-threshold stimulus (bold line 1) or over threshold stimulus (bold line 2) are shown for (**A**) active Src fractions, s_1 (black) and s_2 (blue), and (**B**) partially active fraction s (black) and inactive fraction s_i (blue). At time t_0 = 5 s (marked by arrow), the rate constant k_1 was increased from the initial level of 0.03 to 0.1 s^{-1}. After time $t_1 = t_0 + 1$ s (bold line 1) or $t_2 = t_0 + 1.5$ s (bold line 2), k_1 was decreased to the initial level. Responses to sub-threshold and over-threshold stimuli are shown by dashed and solid lines, respectively. **C.** The trajectory (red) that corresponds to the over-threshold time-dependent response, the Z-shaped QSS curve (black) and two QSS curves (blue) for k_1 = 0.03 s^{-1} (curve 1) and 0.1 s^{-1} (2) are shown in the plane of the inactive and active Src fractions (s_i and s_1). The other parameters are the same as in Fig. 4 of the main text (k_2=0.01, k_3=20, k_4=1, k_5=2, k_6=1, k_7=1 (s^{-1}), β=0.01, δ=0.05, ξ=1).

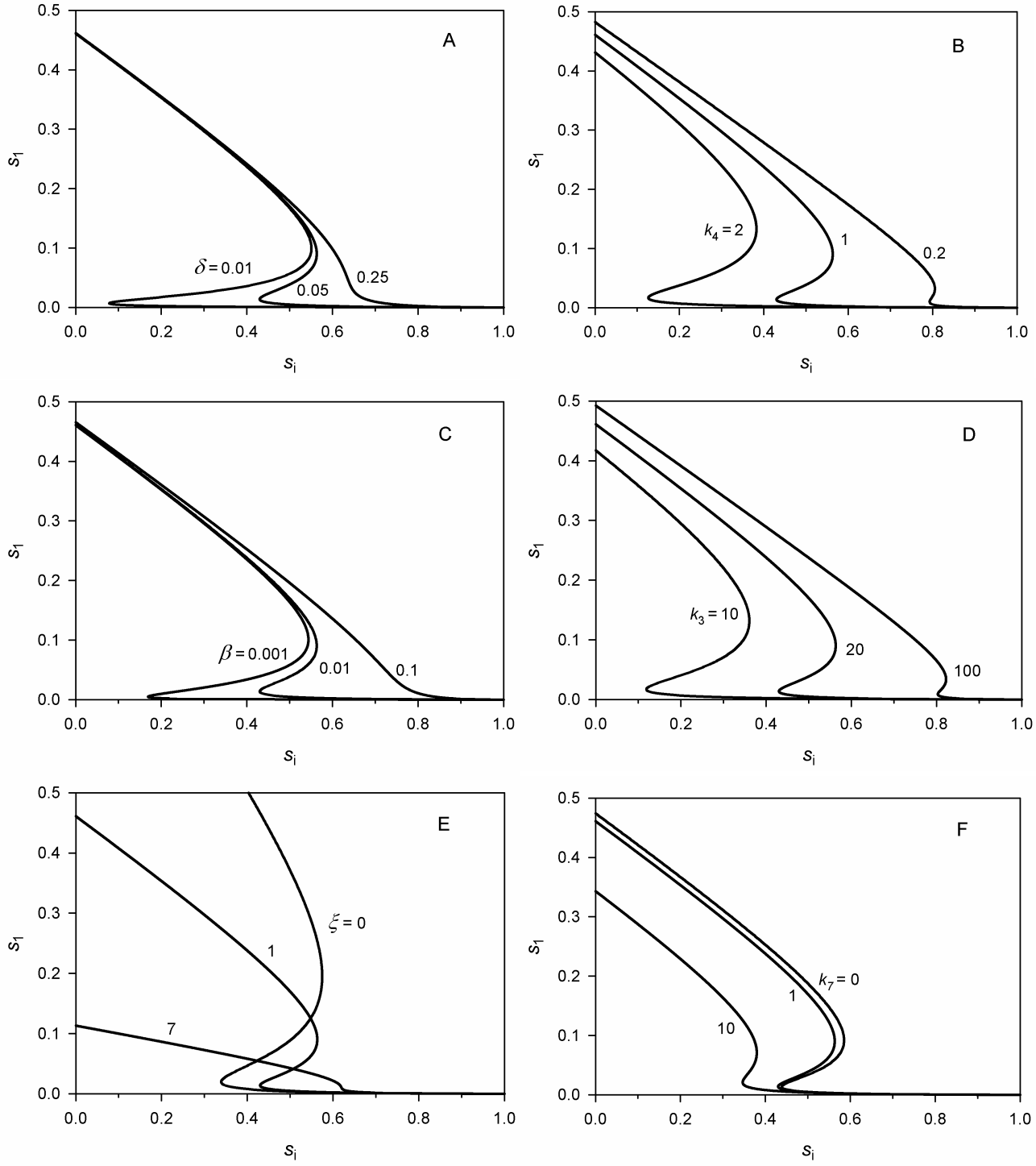

Fig. S3. Complete numerical investigation of the dependence of the Z-shaped QSS curve on each kinetic parameter involved. The OSS curve considered is determined by Eq. 10 of the main text and depends on six kinetic parameters out of nine kinetic parameters of the Src cycle (see Eqs. 6-8 of the main text). Panels **A – F** show the QSS dependencies on the following parameters **A** – δ, **B** – k_4, **C** – β, **D** – k_3, **E** – ξ, **F** – k_7. For each panel, fixed parameter values are the same as in Fig. S1.

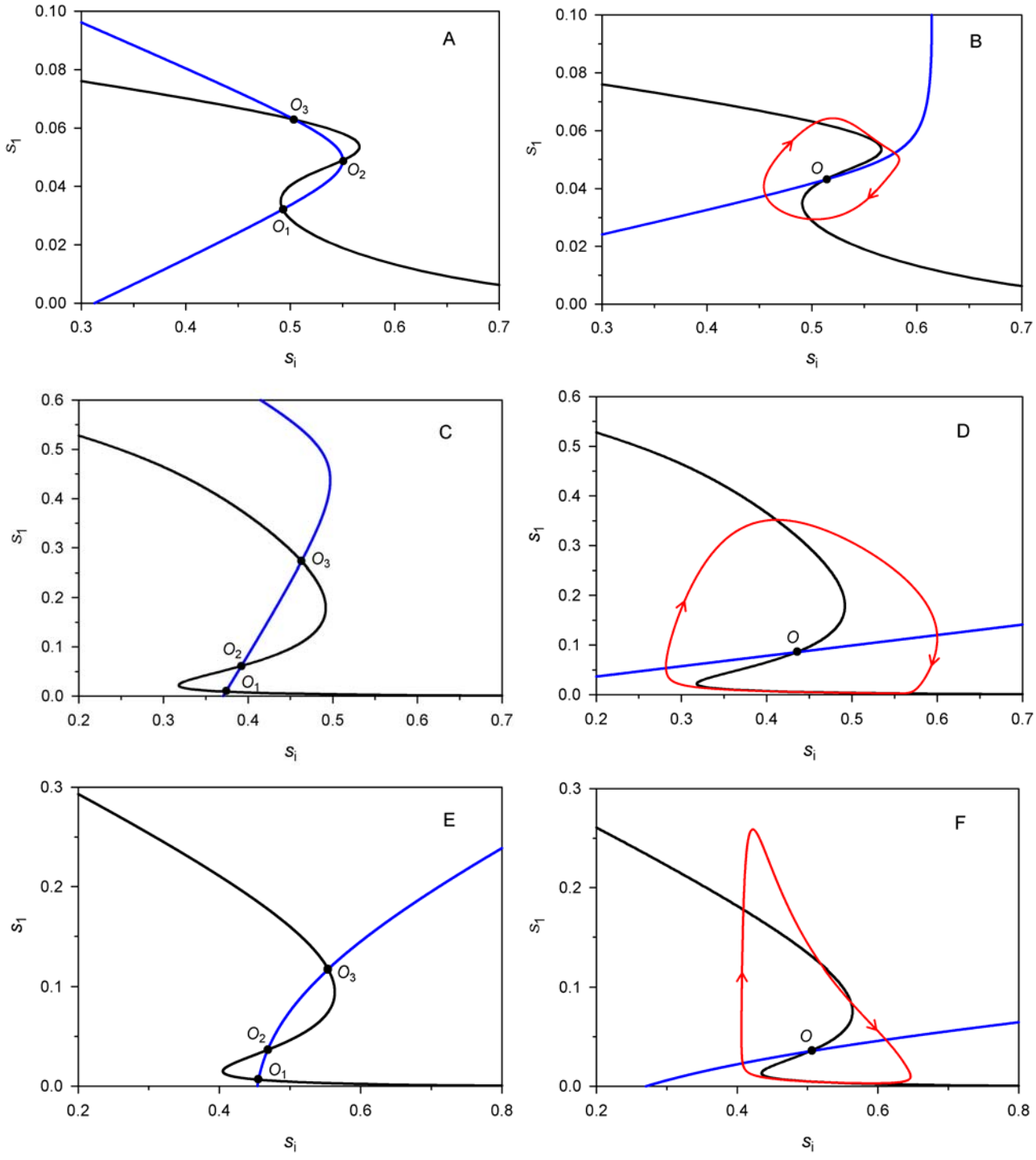

Fig. S4. Effects of saturabilities of reaction rates on the QSS dependencies. Panels **A** and **B** show that the saturability of rate v_7 instead of rate v_4 keeps bistable and oscillatory Src behavior. When $v_4 / S^{tot} = k_4 s_1$ and $v_7 / S^{tot} = k_7 s_2 / (\beta_7 + s_2)$, the first QSS curve (described by Eq 10 in the main text) is expressed as, $s_i = \left(f_1 - \sqrt{f_1^{\,2} - 4\delta f_2}\right) / 2\delta$, and can still maintain a Z shape. The second QSS curve is no longer linear (cf. Eq 11), being expressed as, $s_i = \left(k_2(1 - s_1 - s_2) + v_7 / S^{tot}\right) / (k_1 + k_2)$, where

$f_1 = 2\delta + (1-2\delta)(s_1 + s_2)$, $f_2 = (1 - s_1 - s_2)\left(\delta + (1-\delta)(s_1 + s_2)\right) - (v_4 + v_7)/S^{tot}k_3$, and quasi-steady-state s_2 equals to, $s_2 = \left((k_5 s_1 - k_6\beta_7 - k_7) + \sqrt{(k_5 s_1 - k_6\beta_7 - k_7)^2 + 4k_5 k_6 \beta_7 s_1}\right)/2k_6$. **A**. Three steady states (stable O_1 and O_3 and unstable O_2) demonstrate the existence of bistability. k_1=2.2, k_2=1 (s^{-1}). **B**. A **s**ingle unstable steady state (O) surrounded by a limit cycle (red), which corresponds to stable oscillatory pattern of Src activity at k_1=1.6, k_2=0.01 (s^{-1}). For both panels **A** and **B**, k_4=1, k_5=20, k_7=1 (s^{-1}), β_7=0.01; the remaining parameters are given in the legend to Fig. 2C of the main text. **C** and **D.** Saturable v_4 and v_7, $v_4/S^{tot} = k_4 s_1/(\beta + s_1)$, $v_7/S^{tot} = k_7 s_2/(\beta_7 + s_2)$, k_4= k_7=1 s^{-1}, β=β_7 = 0.01. Designations are the same as in **A** and **B**. **C**, k_1=1.7, k_2=1 (s^{-1}). **D**, k_1=0.4, k_2= 0.01 (s^{-1}). The remaining parameters are the same as for panels **A** and **B**. **E** and **F**. Saturable RPTP-catalyzed rates $v_1/S^{tot} = k_1 s_i/(\beta_1 + s_i)$ and $v_6/S^{tot} = k_6 s_2/(\beta_6 + s_2)$. The Z-shaped QSS curve is given by the same equations as for **A**, **B**. The second QSS curve is given as, $s_i = \left((f_3 - k_1 - k_2\beta_1) + \sqrt{(f_3 - k_1 - k_2\beta_1)^2 + 4k_2\beta_1 f_3}\right)/2k_2$, where $f_3 = k_2(1 - s_1 - s_2) + k_7 s_2$ and $s_2 = \left((k_5 s_1 - k_7\beta_6 - k_6) + \sqrt{(k_5 s_1 - k_7\beta_6 - k_6)^2 + 4k_5 k_7 \beta_6 s_1}\right)/2k_7$. β_1 = β_6 = 0.1 **E**, k_1= k_6=0.22, k_2= 0.33 (s^{-1}). **F**, k_1= k_6=0.1, k_2= 0.1 (s^{-1}). The remaining parameters are the same as for **A** and **B**.

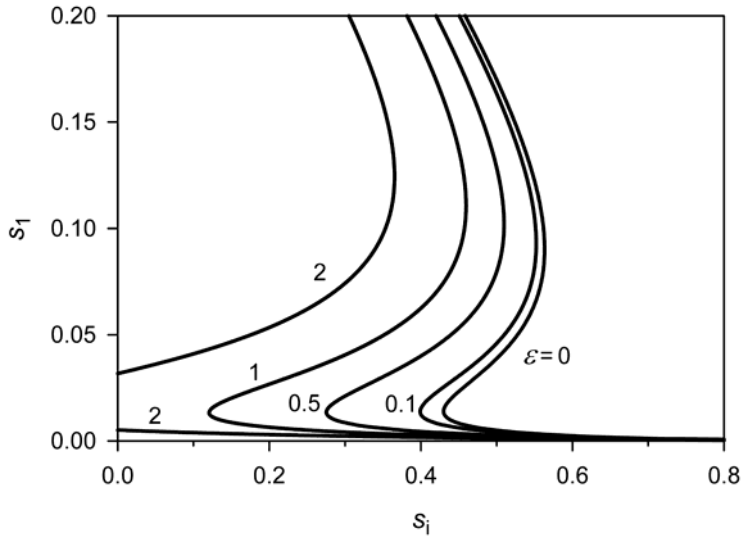

Fig. S5. Effects of large concentrations of Src dimers on the QSS dependence. A family of Z-shaped QSS curves that correspond to increasing Src intermolecular interaction affinities and concentrations of Src dimers in autophosphorylation step 3. When concentrations of Src dimers are taken into account, the expression of partially active fraction s in terms of the remaining fractions, s_i, s_1 and s_2, is no longer linear, but satisfies the following quadratic equation, $1 = s_i + s(1+\varepsilon_0 s) + s_1(1+\varepsilon_1 s) + s_2(1+\varepsilon_2 s)$, where $\varepsilon_0 = S^{tot}/K_S$, $\varepsilon_1 = S^{tot}/K_{a1}$, $\varepsilon_2 = S^{tot}/K_{a2}$. The solution to this equation is the following, $s = \left(-(1+\varepsilon_1 s_1 + \varepsilon_2 s_2) + \sqrt{(1+\varepsilon_1 s_1 + \varepsilon_2 s_2)^2 + 4\varepsilon_0(1-s_i-s_1-s_2)}\right)/2\varepsilon_0$. Accordingly, Eq. 10 for the QSS curves is replaced by the equation, $k_3 s(\delta s + (1+\xi)s_1) - k_4 s_1/(\beta + s_1) - k_7 \xi s_1 = 0$, the solutions to which are shown for increasing values of $\varepsilon = \varepsilon_0 = \varepsilon_1 = \varepsilon_2$, indicated near each curve. The other parameters are the same as in Fig. S1.

Toggle switches, pulses and oscillations are intrinsic properties of the Src activation/deactivation cycle

Nikolai P. Kaimachnikov[1,2] and Boris N. Kholodenko[1,3*]

[1] Department of Pathology, Anatomy and Cell Biology, Thomas Jefferson University, Philadelphia, PA, USA
[2] Institute of Cell Biophysics, Russian Academy of Sciences, Pushchino, Moscow region, Russia.
[3]Systems Biology Ireland, University College Dublin, Belfield, Dublin, Ireland

[*]**Corresponding author**
Boris N. Kholodenko
E-mail: Boris.Kholodenko@ucd.ie

Running Title
Switches, pulses and oscillations in Src signaling

Abbreviations
Csk, C-terminal Src kinase; FAK, focal adhesion kinase; QSS, quasi steady-state; PTP1B, protein tyrosine phosphatase 1B; RPTP, receptor-type protein tyrosine phosphatase; RTK, receptor tyrosine kinase; SFK, Src-family kinase; SH2, Src homology 2; SH3, Src homology 3, Y – tyrosine residue.

Key words
signaling dynamics; kinetics; bistability; oscillations, excitable behavior; Src-family kinases; autophosphorylation

Subdivision
Systems biology

Abstract

Src-family kinases (SFKs) play a pivotal role in growth factor signaling, mitosis, cell motility and invasiveness. In their basal state, SFKs maintain a closed autoinhibited conformation where the Src homology 2 domain interacts with an inhibitory phosphotyrosine in the C-terminus. Activation involves dephosphorylation of this inhibitory phosphotyrosine, followed by intermolecular autophosphorylation of a specific tyrosine residue in the activation loop. The spatiotemporal dynamics of SFK activation controls cell behavior, yet this dynamics remains largely uninvestigated. Here we show that the basic properties of the Src activation/deactivation cycle can bring about complex signaling dynamics including oscillations, toggle switches and excitable behavior. These intricate dynamics do not require imposed external feedback loops and occur at constant activities of Src inhibitors and activators, such as C-terminal Src kinase (Csk) and receptor-type protein tyrosine phosphatases (RPTP). We demonstrate that underexpression/mutations of Csk or simultaneous overexpression of Csk and RPTP can transform Src response patterns into oscillatory or bistable responses, respectively. Likewise, Src overexpression leads to dysregulation of Src activity promoting sustained self-perpetuating oscillations. Distinct types of responses can allow SFKs to trigger different cell-fate decisions where cellular outcomes are determined by the stimulation threshold and history. Our mathematical model helps to understand puzzling experimental observations and suggests conditions where these different kinetic behaviors of SFKs can be tested experimentally.

Introduction

Members of the Src-family tyrosine kinases (SFKs) are expressed in essentially all vertebrate cells and regulate pivotal cellular processes, such as cytoskeleton rearrangements and motility, initiation of DNA synthesis pathways, cell differentiation, mitosis and survival. SFKs are stimulated by a multitude of cell-surface receptors, including receptor tyrosine kinases (RTKs) and phosphatases, integrins, cytokine receptors and G-protein coupled receptors. Activated SFKs phosphorylate different effectors, such as the focal adhesion kinase, small GTPases (Rho, Rac and Cdc42), and phospholipase Cγ, thereby acting as critical switches of downstream pathways [1, 2]. Related to the central roles of SFKs in cellular regulation, their aberrant signaling leads to cell transformation [3]. However, despite the *src* gene was the first oncogene to be discovered and the Src kinase has been studied for many years, the SFK signaling dynamics and its role in cell physiology and diseases, such as cancer, is not yet understood [4, 5].

All SFKs have common structural and regulatory features. Here, we will not distinguish between different family members, but rather explore generic properties of their complex signaling dynamics. Two tyrosine (Y) residues are critical regulators of SFKs: (*i*) the inhibitory site Y_i located at the C-terminal (Y527/530 for chicken/human c-Src and Y507 for Lyn) and (*ii*) activatory site Y_a (Y416/419 for chicken/human c-Src and Y396 for Lyn) located within the activation loop in the catalytic domain. Phosphorylation of Y_i promotes an autoinhibited conformation, whereas autophosphorylation of Y_a correlates with high kinase activity [6-8]. In the case of c-Src, Y_i is phosphorylated by the C-terminal Src kinase (Csk) and its homolog Chk. Reduced Csk expression was suggested to play a role in Src activation in human cancer [5]. Receptor-type protein tyrosine phosphatases (RPTPs), including PTPα, PTPλ and PTPε, can dephosphorylate Y_i, leading to Src activation [9-12]. Cytoplasmic phosphatases, such as protein tyrosine phosphatase 1B (PTP1B) and the Src homology 2 (SH2) domain-containing phosphatases (SHP1/2) can also activate Src, although less effectively than RPTPs [5, 7]. Other Src activators, such as phosphorylated RTKs can bind the Src SH2 domain, facilitating dephosphorylation of the inhibitory tyrosine pY_i. The phosphatases that dephosphorylate the activating site pY_a include the C-terminal site phosphatases, as well as others, such as PTP-BL [2]. In addition, all SFKs have other phosphorylation sites, which can alleviate intramolecular interactions that lead to an autoinhibited conformation [2].

SFKs can associate with the plasma membrane and intracellular membranes, such as the endoplasmic reticulum, endosomes and other structures. Myristoylation of the N-terminal is necessary, but not sufficient for the membrane localization, which also requires SFK basic residues. For myristoylated SFKs that lack such basic residues, membrane localization is shown to be additionally facilitated by post-translational palmitoylation [13]. Although recruitment of doubly acylated SFKs into lipid rafts and caveolae was reported [13, 14], whether this Src localization is predominant remains controversial.

SFKs can display a variety of temporal activity patterns, differentially controlling the cell behavior. For instance, growth factor stimulation may lead to a transient or sustained SFK activity, whereas the assembly and disassembly of focal adhesions during cell migration, mediated by integrin receptors involves periodic Src activation and deactivation [5, 15], and periodic SFK activation was also reported in the cell cycle [16]. These complex dynamics might be explained by multiple feedback loops, since SFKs can phosphorylate their regulators, affecting their catalytic activities. Recent theoretical models by Fuss *et al* [17-19] incorporated positive feedback that can occur owing to Src-induced phosphorylation and activation of PTPα, and negative feedback that is exerted via the Csk-binding protein Cbp, which when phosphorylated by SFKs can target Csk to Src, promoting inhibitory phosphorylation of Src. These feedback loops may induce the complex dynamic behaviors of both Src kinases and their effectors and regulators. For instance, the positive feedback loop mediated by PTPα can result in abrupt switches of Src kinase between low and high activity states which may explain the activation of Src during mitosis [17]. Such a system that switches between two distinct stable states, but cannot rest in intermediate states, is termed bistable, and there has been emerging interest in bistability as a ubiquitous and unifying principle of cellular regulation [20-23]. We show here that Src cycle bistability arises merely from intermolecular autophosphorylation, a salient feature of many protein kinases [24-26]. Other dynamic regimes brought about by external feedback loops included excitable behavior where a transient stimulation causes Src activity to overshoot before it returns to the basal level, as well as oscillations [17-19]. Autocatalytic phosphorylation of the focal adhesion kinase (FAK) together with FAK-Src reciprocal activation was predicted to result in switch-like amplification of integrin signaling, and also, under assumption of rapid FAK synthesis and degradation, in slow oscillations of FAK activity [27].

The present paper shows that extremely complex dynamic behaviors can be brought about by the intrinsic properties of the minimal Src activation/deactivation cycle in the absence of any external regulatory loops (in contrast to earlier conclusions [17]). Using computational modeling to elucidate these dynamic properties, we demonstrate that SFK can display oscillatory, bistable and excitable behaviors. We show that overexpression or mutation of SFKs (or their activators/inhibitors) do not merely change the amplitude of responses to external stimuli, but dramatically transform the response dynamics. For instance, when Csk activity is suppressed, a transient stimulus, which normally causes a transient Src activation (in the stable low-activity regime), can bring about oscillatory Src activity patterns or, when Csk and RPTP activities are in the proper regions, abrupt switches to a sustained, high Src activity state (within the bistable domain). Our findings unveil the intrinsic complexity of the Src dynamics and allow for direct experimental testing.

Results

Kinetic analysis background: basic properties of the Src activation/deactivation cycle.

Kinetic scheme of the Src cycle. Src activity is regulated by intramolecular and intermolecular interactions that are controlled by tyrosine phosphorylation [15, 28]. If the negative-regulatory tyrosine residue Y_i is phosphorylated, whereas the activatory residue Y_a is dephosphorylated, Src is catalytically inactive. In this autoinhibited conformation, the SH2 domain binds to pY_i on the C-terminal tail, and the SH3 domain binds to the linker between the SH2 and kinase domains at the back of the small lobe preventing the formation of a productive catalytic cleft [29]. Thus, these interactions clamp the kinase domain in an inactive conformation [30]. We will refer to this inactive Src form as $S_i(pY_i, Y_a)$ or simply S_i (Fig. 1). Under the basal condition *in vivo*, 90 - 95% of Src can be in this dormant state [12]. Dephosphorylation of pY_i by transmembrane phosphatases (PTPα, PTPλ or PTPε) or by cytoplasmic phosphatases yields the partially active form S where both sites Y_i and Y_a are dephosphorylated, $S(Y_i, Y_a)$ [31]. This reaction is shown as step 1 in the kinetic scheme presented in Fig. 1. Phosphorylation of S on Y_i by Csk inactivates S yielding S_i (step 2, Fig. 1).

A hallmark of the Src kinetic cycle is autophosphorylation of the activation site Y_a, which was reported to be intermolecular catalysis [28, 32]. This is shown as step 3, which yields the fully active form $S_{a1}(Y_i, pY_a)$. Phosphatases, including PTP1B dephosphorylate pY_a and convert S_{a1} back to S (step 4). For at least two SFKs (Src and Yes), it was reported that autophosphorylation

prevents deactivation, but not phosphorylation of S_{a1} by Csk [5, 7]. Step 5 in Fig. 1 is phosphorylation of S_{a1} on site Y_i resulting in the dually phosphorylated form $S_{a2}(pY_i, pY_a)$ with the catalytic activity comparable to that of S_{a1} [7, 8, 33]. Dephosphorylation on pY_i or pY_a converts S_{a2} into S_{a1} (step 6) or S_i (step 7), respectively. The transition from the catalytically inactive form $S_i(pY_i, Y_a)$ to dually phosphorylated form $S_{a2}(pY_i, pY_a)$ was not observed [7], and there is no such reaction in Fig. 1. The resulting kinetic scheme consists of two cycles of opposing activation/deactivation reactions (steps 1 - 4) and a "bypass" from an active S_{a1}/S_{a2} conformation to an inactive S_i conformation (steps 5 - 7); a structure that hints at the complex input-output dynamics [34].

Kinetic equations. The rates of reactions catalyzed by "external" phosphatases and kinases (Fig. 1) are described by Michaelis-Menten type expressions. When the Michaelis constant for a particular reaction of the SFK (de)activation cycle is substantially larger than the concentration of the corresponding SFK form (or the total SFK abundance), the rate is approximated by a linear expression. Although a detailed description at the level of elementary steps that uses the mass-action kinetics would be more precise, it would require a much greater number of variables and unknown parameters. Importantly, the complex Src cycle dynamics demonstrated in the current paper holds true for a mass-action description of all elementary steps.

Using a model, we will delineate essential features that generate bistability, sustained oscillations or excitable behavior of Src temporal responses. Interestingly, these essential properties arise largely from the interaction circuitry of the Src (de)activation cycle and not only from the reaction kinetics. A critical nonlinearity is brought about by intermolecular autophosphorylation of Y_a on S. Any of partially or fully active Src forms, S, S_{a1} or S_{a2}, can catalyze this reaction (step 3, Fig. 1), which involves the following processes,

$$\begin{aligned} \mathrm{S} + \mathrm{S} &\underset{k_S^r}{\overset{k_S^f}{\rightleftharpoons}} \mathrm{S}\cdot\mathrm{S} \xrightarrow{k_S^{cat}} \mathrm{S} + \mathrm{S}_{a1} \\ \mathrm{S}_{a1} + \mathrm{S} &\underset{k_{a1}^r}{\overset{k_{a1}^f}{\rightleftharpoons}} \mathrm{S}_{a1}\cdot\mathrm{S} \xrightarrow{k_{a1}^{cat}} \mathrm{S}_{a1} + \mathrm{S}_{a1} \\ \mathrm{S}_{a2} + \mathrm{S} &\underset{k_{a2}^r}{\overset{k_{a2}^f}{\rightleftharpoons}} \mathrm{S}_{a2}\cdot\mathrm{S} \xrightarrow{k_{a2}^{cat}} \mathrm{S}_{a2} + \mathrm{S}_{a1} \end{aligned} \qquad (1)$$

The autophosphorylation rate (v_3) is the sum of the rates catalyzed by each form. Applying quasi-steady-state approximation for the intermediate complexes, we obtain a simple expression for v_3,

$$v_3 = \left(\frac{k_S^{cat}}{K_S}[\mathrm{S}] + \frac{k_{a1}^{cat}}{K_{a1}}[\mathrm{S_{a1}}] + \frac{k_{a2}^{cat}}{K_{a2}}[\mathrm{S_{a2}}] \right)[\mathrm{S}] \,, \tag{2}$$

where $k_S^{cat}, k_{a1}^{cat}, k_{a2}^{cat}$ and $K_S = (k_S^r + k_S^{cat})/k_S^f$, $K_{a1} = (k_{a1}^r + k_{a1}^{cat})/k_{a1}^f$, $K_{a2} = (k_{a2}^r + k_{a2}^{cat})/k_{a2}^f$ are the catalytic and Michaelis constants, respectively, of component processes involved in step 3. Since the forms $\mathrm{S_{a1}}$ and $\mathrm{S_{a2}}$ were reported to have approximately similar catalytic activities [7, 33], we assume that $k_{a1}^{cat}/K_{a1} \approx k_{a2}^{cat}/K_{a2}$ for illustrative purposes. Notably, Src association with the plasma membrane can lead to a significant increase in the k^{cat}/K_m ratio of intermolecular autophosphorylation, making this ratio larger than such ratios for soluble kinases and phosphatases [35].

Given the rate v_3 nonlinearity that arises from intermolecular interactions (Eq. 2), we next show that the only remaining prerequisite for bistable, excitable and oscillatory Src responses is the saturability of step 4 or/and steps 5 or 7 (regardless whether step 3 is far from saturation or not). Because recent evidence indicates that PTP1B activity can be saturable in live cells [36], we will first assume the saturability of step 4 (as a minimal requirement for the complex dynamics) and consider other nonlinear rate dependencies later. Together with Eq. 2, the rate expressions for a basic model are described as follows,

$$v_1 = k_1[\mathrm{S_i}], \quad v_2 = k_2[\mathrm{S}], \quad v_4 = \frac{V_4^{\max}[\mathrm{S_{a1}}]}{K_4 + [\mathrm{S_{a1}}]}, \quad v_5 = k_5[\mathrm{S_{a1}}], \quad v_6 = k_6[\mathrm{S_{a2}}], \quad v_7 = k_7[S_{\mathrm{a2}}]. \tag{3}$$

The first-order rate constants, k_1, k_2, k_5, k_6 and k_7, approximate the $k^{cat}[\mathrm{E}]/K_M = V^{\max}/K_M$ ratios for the corresponding enzyme reactions and have dimension of 1/time. Although linear approximation of the enzyme rate allows lumping three parameters k^{cat}, [E] and K_M into the apparent first-order constant, below we also use the enzyme concentrations, such as [RPTP], [Csk] and [PTP1B], as parameters that mirror stimulation or changes in the external conditions.

We consider the time scale on which the total Src concentration (S^{tot}) is conserved. Neglecting the concentrations of dimers, $\mathrm{S}\cdot\mathrm{S}$, $\mathrm{S_{a1}}\cdot\mathrm{S}$, $\mathrm{S_{a2}}\cdot\mathrm{S}$, i.e. assuming unsaturated condition for step 3

(this simplifying assumption is relaxed below), [S] is expressed as a linear combination of the following independent concentrations,

$$[\mathrm{S}] = S^{tot} - [\mathrm{S_i}] - [\mathrm{S_{a1}}] - [\mathrm{S_{a2}}]. \quad (4)$$

It is convenient to introduce dimensionless concentrations equal to the relative fractions of Src in each form,

$$s_\mathrm{i} = [\mathrm{S_i}]/S^{tot}, \quad s = [\mathrm{S}]/S^{tot}, \quad s_1 = [\mathrm{S_{a1}}]/S^{tot}, \quad s_2 = [\mathrm{S_{a2}}]/S^{tot} \quad (5)$$

The conservation of the total Src concentration (Eq. 4) leaves only three independent variables in the kinetic scheme of Fig. 1, and using Eqs. 2-5 allows describing Src dynamics as follows,

$$\frac{ds_\mathrm{i}}{dt} = \frac{v_2 - v_1 + v_7}{S^{tot}} = k_2(1 - s_\mathrm{i} - s_1 - s_2) - k_1 s_\mathrm{i} + k_7 s_2 \quad (6)$$

$$\frac{ds_1}{dt} = \frac{v_3 - v_4 + v_6 - v_5}{S^{tot}} = k_3\left(1 - s_\mathrm{i} - s_1 - s_2\right)\left(\delta(1 - s_\mathrm{i} - s_1 - s_2) + s_1 + s_2\right) - \frac{k_4 s_1}{\beta + s_1} + k_6 s_2 - k_5 s_1 \quad (7)$$

$$\frac{ds_2}{dt} = \frac{v_5 - v_6 - v_7}{S^{tot}} = k_5 s_1 - (k_6 + k_7) s_2 \quad (8)$$

$$k_3 = \frac{k_{a1}^{cat}}{K_{a1}} S^{tot}, \quad \delta = \frac{k_S^{cat}}{K_S} / \frac{k_{a1}^{cat}}{K_{a1}}, \quad k_4 = V_4^{\max}/S^{tot}, \quad \beta = K_4/S^{tot}.$$

Note that a completely dimensionless differential equation system can be obtained by introducing dimensionless rates (w) and time (τ), for instance, as follows, $\omega_i = v_i / V_4^{\max}$, $\tau = k_4 t$. Although this reduces the number of parameters by one (giving a minimal number of independent parameter combinations), perturbation to the rate of a single step, $V_4^{\max}$, will change many other parameters, and for clarity of the exposition we present the analysis of the Src cycle in terms of Eqs. (6)-(8).

Intrinsic regulatory properties of the Src (de)activation cycle responsible for toggle switches and oscillations. Available experimental data show wide ranges of kinetic parameters for the kinases and phosphatases that catalyze the Src cycle reactions (Supplementary Table S1) and warrant a detailed exploration of Src responses under various conditions that encompass the vast parameter space. Variation of the apparent first-order rate constants k_1 and k_2 mimic Src activation and deactivation. These (de)activation processes are brought about by stimulation of a plethora of cellular receptors and signaling pathways. For instance, following growth factor stimulation, the SH2 domain of SFK can bind to phosphotyrosines on activated RTKs [37]. This releases the intramolecular association of the SFK SH2 domain with an inhibitory

phosphotyrosine (pY_i) in the C-terminus, facilitating pY_i dephosphorylation, which is modeled as an increase in k_1. Likewise, other SH2 and SH3 domain-containing proteins that are recruited to the membrane by activated receptors can interact with pY_i, alleviating intramolecular inhibition of SFK [2, 38]. The changes in the active RPTP and Csk fractions correspond to varying rate constants k_1, k_6 and k_2, k_5, respectively (Fig. 1). The model takes into account that the apparent first-order rate constant (k_3) of intermolecular phosphorylation step is greater than the other first-order rate constants owing to the Src membrane localization [35].

A central result of this paper is that the complex dynamics of Src responses can be understood in terms of a simple basic model of the Src (de)activation cycle in the absence of any imposed external feedback. To explain how toggle switches (bistability) and oscillations arise, we will first examine the steady-state properties of the Src cycle. The analysis can be perceived readily, if we plot two quasi steady-state (QSS) dependencies of variables (which are the relative Src fractions) on one plane. This graphical representation is useful, since all steady states of the Src cycle correspond to the points where these curves intersect. For instance, we can immediately detect bistability, as the case when these curves intersect in three different points. We will consider two of three independent variables under stationary conditions, whereas the remaining variable changes with time. Because of the algebraic structure of Eqs. 6-8, it is convenient to consider the variable s_2 at steady state for each of the two QSS curves, where either s_i or s_1 are allowed to change. Equating the time derivative in Eq. 8 to zero ($ds_2/dt = 0$), s_2 is expressed in terms of s_1, as follows:

$$s_2 = \xi s_1, \qquad \xi = k_5/(k_6+k_7). \tag{9}$$

We will see now that nonlinearities of the rates v_3 (brought about by intermolecular interactions) and v_4 lead to a Z-shaped QSS dependence of the active Src fraction (s_1 or s_2) on the inactive fraction (s_i). After substitution of Eq. 9 into Eq. 7 and equating the time derivative to zero ($ds_1/dt = 0$), we obtain a quadratic equation, which determines the first QSS curve,

$$k_3\left(1 - s_i - (1+\xi)s_1\right)\left(\delta(1-s_i) + (1-\delta)(1+\xi)s_1\right) - \frac{k_4 s_1}{\beta + s_1} - k_7 \xi s_1 = 0. \tag{10}$$

The solution to this quadratic equation is given in the legend to Supplementary Fig. S1. A simple graphical analysis shows that up to three different s_1 values can correspond to a single s_i value. This Z-shaped plot of this first QSS curve, s_1 versus s_i, is illustrated in Fig. 2 (see also Fig.

S1). The second QSS curve is obtained from the condition $ds_i / dt = 0$ (Eq. 6). Since in our basic model both Eqs 6 and 9 are linear, this QSS curve is a straight line on the s_i, s_1 plane, Fig. 2 (nonlinear case is considered in a separate section),

$$s_1 = as_i - b, \quad a = \frac{k_1 + k_2}{k_7\xi - k_2(1+\xi)}, \quad b = \frac{k_2}{k_7\xi - k_2(1+\xi)} \ . \tag{11}$$

The slope of this line can be positive or negative, depending on the interrelationship between the rate constants of the following steps in Fig. 1, S → S_i (k_1), S_{a1} ↔ S_{a2} (k_5, k_6), and S_{a2} → S_i (k_7). The slope is positive, when

$$1/k_2 > 1/k_7 + 1/k_5 + k_6/k_5k_7 \,, \tag{12}$$

and it is negative otherwise. It was reported that autophosphorylation facilitates the phosphorylation of SFK by Csk [39, 40], implying that $1/k_2 > 1/k_5$ (Fig. 1). Therefore, at least for sufficiently large k_7 (PTP1B concentrations), Eq. 12 is satisfied, resulting in a positive slope of the second QSS curve.

Fig. 2 shows that there can be from one (O) to three (O_1, O_2, O_3) points of intersection between the two QSS curves (a Z-shaped and linear), which present all steady states of the Src cycle. When there are three intersections, the steady state O_1 at the lower branch of the Z-shaped curve (low Src activity) and the state O_3 at the upper branch (high Src activity) are both stable, whereas the intermediate state O_2 is unstable (Fig. 2A and 2B). While at the stable lower or upper steady-state branches of the Z-shaped curve, Src behaves as a toggle switch that responds abruptly to gradually increasing or decreasing stimuli. In Fig. 3, the stimulus is presented as a series of relatively small, stepwise changes in the active level of receptor-type phosphatase RPTP (indicated by numbers 1-3). The initial increase in [RPTP] from level 1 to 2 leads to a small increase in the Src activity, which remains low (at the lower branch of the steady-state dependence of Src activity on [RPTP], Fig. 3A). The next incremental increase in [RPTP] to level 3 that is higher than a critical value, corresponding to point P_1 in Fig. 3A (called the turning point), changes Src activity dramatically. The time course (Fig. 3B) shows a rapid jump (with an overshoot) from the low-activity branch in Fig. 3A (Off state) to the high-activity branch (On state). Importantly, the reversal of stimulus to level 2 does not return the Src activity to its Off state. Bistable systems always display hysteresis, meaning that the stimulus must exceed a threshold to switch the system to another steady state, at which it may remain, when the stimulus decreases. To return to the initial Off state, [RPTP] should decrease below the critical value that corresponds to turning point P_2 in Fig. 3A. Thus, Src

activity can be high or low under the exactly same condition depending on whether the stimulus was higher or lower than the threshold (the stimulation history). Likewise, bistable switches in Src activity may be observed for gradual changes in active Csk concentration.

When there is only one point of intersection between the two QSS curves and thus, one steady state, this state can be either stable or unstable. Depending on the stimulation level and other conditions, in a stable steady state Src activity can be low or high (Figs. 2A and 2B). In the resting state *in vivo*, Src activity is very low, $s_i \approx 0.9 - 0.95$ [12]. Increase in the stimulus level can gradually increase Src activity, or transfer the system into a bistable domain, where a further increase in the stimulus results in a switch-like change in Src activity. When the condition expressed by Eq. 12 holds true (i.e., the slope of the second QSS curve is positive), a single steady state can be unstable, surrounded by a limit cycle (Fig. 2C), which corresponds to sustained oscillations in Src activity (Fig. 3C and 3D). Toggle switches in Src activity are likely to occur when the activities of both activatory phosphatase (RPTP) and inhibitory kinase (Csk) are high, whereas Src oscillations may occur when these activities are low (see Figs. 2 and 3 and, in more detail, below). Close to this stable oscillatory pattern, a stepwise increase in stimulus can lead to oscillations, whereas at higher RPTP and Csk activities such an increase triggers switch-like behavior.

Src excitable behavior in response to transient stimuli.

Under proper conditions, a single stable steady state with low basal Src activity can become excitable. In this case, the Src protein behaves as an excitable device with a built-in excitability threshold. Depending on the magnitude and duration of a transient stimulus, Src activation responses fit into one of two distinct classes of either low or high amplitude responses, whereas there are no intermediate responses, merely proportional to the stimulus. Fig. 4A shows that if the duration of a step-like increase in the stimulus (k_1) is below a critical threshold value, the magnitude of Src response is low. In this case, following a small raise, active Src fractions (s_1 and s_2) remain near the basal state. If the stimulus duration exceeds the threshold value, a large overshoot in Src activity occurs before it returns to the low, basal state.

Fig. 4B helps us understand this excitable behavior by presenting the pulse of Src activity in the plane of the inactive and active fractions, s_i and s_1. If the duration of the stimulus exceeds the critical value, the trajectory in the (s_i, s_1) plane (shown in red) passes the turning point at the lower branch of the Z-shaped QSS curve (shown in black). Since its intermediate branch harbors

unstable states, the trajectory makes an overshoot, yielding a high-amplitude response. Instructively, this also explains a relatively large lag period for the Src activity spike to occur (Fig. 4A), as the basal state of Src at the lower branch (point 1) is far from the turning point. If the initial Src state is closer to the turning point, both the threshold stimulus duration and lag period become shorter (Supplementary Fig. S2). In this case, there is also a recovery period. After the pulse amplitude decreases, the same stimulus cannot excite the system again, until the trajectory returns to the initial state. Sub-threshold durations of the stimulus give low-amplitude responses, because trajectories remain near the lower branch of stable steady states. Interestingly, this excitable behavior of the solutions of Src kinetic equations parallels, on a different time scale, the dynamics of the solutions to the classical Hodgkin-Huxley and FitzHugh-Nagumo equations that describe neural excitation and firing of neuron impulses.

Fig. 4C illustrates Src excitable behavior in response to perturbations to the initial concentrations of the active form (which could correspond to an *in vitro* experiment where a small amount of activated Src is added to the medium). Similarly to parameter perturbations, sub-threshold changes in the active Src concentration yield small amplitude responses, whereas any perturbation that exceeds the threshold results in a large response with almost standard, high amplitude. This over-threshold excitation leads to a large excursion of the trajectory in the (s_i, s_1) plane, before returning to the initial steady state (Fig. 4D).

A pulse of Src activity, which is pivotal for mitosis, can be explained by Src excitability that follows gradual activation by cyclin-dependent kinases [16, 41]. Activation of Src kinases initiates signaling pathways that are required for DNA synthesis. Therefore, the Src excitable behavior, which yields either a low-activity response or high-activity pulse, responding to stimuli under or over threshold, respectively, can be implicated into cell-fate decision processes [42].

Revealing different types of Src dynamics by partitioning the parameter space.

The dynamic behavior of the Src cycle in relationship to various kinetic parameters can be conveniently described by dividing a plane of two selected parameters into areas, which represent different types of dynamic responses. This partitioning of the parameter space helps us perceive how changes in the stimulus, Src activators and inhibitors, and the Src abundance affect the basal low activity state of Src and bring about oscillations, pulses and toggle switches in Src activity.

Fig. 5 shows regions in the plane representing different concentrations of active Csk and RPTP, which correspond to distinct Src dynamics, including monostable, bistable, oscillatory and

excitable behavior. These regions are separated by so-called *bifurcation* boundaries where abrupt, dramatic changes in the steady-state and dynamic behavior of the Src cycle occur. In Fig. 5, these boundaries are determined by two different bifurcations. One is a saddle-node bifurcation where an unstable steady state (termed saddle) merges with another steady state (node). This event corresponds to the abrupt change (presence or absence) of switch-like, bistable behavior [43]. The other is the Hopf bifurcation where a steady state changes its stability, accompanied by the appearance or disappearance of a limit cycle (see Methods). A stable limit cycle presents oscillatory pattern of Src activity, such as shown in Fig. 3C.

A single, stable steady state of Src activity exists within two large areas that are marked by number 1 in the plane of the Csk and RPTP concentrations. Within these two regions of monostability, there are parameter sets where the QSS dependence of the active Src fraction on the inactive fraction given by Eq. 10 becomes monotonically decreasing curve. For instance, this happens for the large ξ values, corresponding to $s_2/s_1 >> 1$, see Eq. 9 and Supplementary Fig. S3E. In this case, changes in the Src activity follow changes in the stimulus, so that an increase or decrease in the stimulus amplitude merely causes Src activity to increase or decrease. However, within other parts of monostable region 1, Src activity displays excitable behavior where similar, high-amplitude responses occur for any stimulus amplitude over a certain threshold (Fig. 4). The next large area, which is marked by 2, corresponds to bistable behavior. In this region there are three steady states, two stable (Off and On) states and one intermediate unstable (saddle) state. A typical biological scenario for an abrupt transition (saddle-node bifurcation) from a single steady state in region 1 to three steady states in region 2 is shown in Fig. 3A, where two new steady states emerge when gradually increasing [RPTP] passes the turning point P_2, whereas Src activity switches to a high state only after [RPTP] passes the turning point P_1 (Fig. 3B). Similarly to region 1, region 2 spreads out to arbitrary large activities of Csk and RPTP, demonstrating robustness of the bistable behavior.

Oscillations occurring within regions 3 and 4 correspond to lower concentrations of active Csk and RPTP than the values that characterize the bistable region. Similarly to bistable regime, oscillatory behavior is robust, although it occupies smaller region in this parameter plane (Fig. 5). In region 3, there is a single unstable steady state, whereas in a smaller region 4 there are three unstable steady states; yet within each region there is a stable limit cycle that surrounds one (region 3) or three (region 4) unstable states, presenting sustained oscillations in Src activity. The

remaining regions 5 and 6 harbor a stable steady state with low or high Src activity, respectively, and two unstable steady states each. In both areas, excitable Src responses to changes in the initial active Src fraction are observed (region 6 is too small to be seen on the scale of Fig. 5).

By crossing the parameter plane parallel to the [RPTP] axis at different constant [Csk], we obtain one-parameter bifurcation diagrams, which present different scenarios of how changes in active RPTP can influence the steady-state magnitudes and dynamics of Src fractions. At relatively low [Csk] = 25 nM, a gradual increase in the stimulus (expressed in terms of active [RPTP]), first leads to a gradual increase in the active Src fraction s_1 and a decrease in the inactive fraction s_i (two left black curves in Fig. 5B). This [RPTP] range corresponds to region 1 (see the dashed line parallel to the [RPTP] axis at [Csk] = 25 nM in Fig. 5A). With further increase in the stimulus, the steady state loses its stability, which coincides with entering region 3 where Src displays oscillatory behavior (parts of black curves shown by dotted line), and then the stationary regime becomes again stable at high [RPTP]. Monotonic and sharply non-monotonic changes in s_1 and s_i, respectively, reflect the progression along a Z-shaped QSS curve in the (s_i, s_1) plane shown in Fig. 2C. A larger variety of Src responses to changes in [RPTP] is observed at higher [Csk], where crossing the parameter plane in Fig. 5A involves entering more regions with different dynamics. For instance, the blue curves (second from the left, Fig. 5B) capture dynamics that corresponds to crossing regions 1, 5, 4, 3 and again region 1 with gradual increase in [RPTP]. Increase in the stimulus first brings about excitable Src behavior and then, when [RPTP] passes the turning point (marked bold), lands the system into the oscillatory domain, whereas with further increase in the stimulus a single steady state regains stability. The remaining curves in Fig. 5B (red and green) display bistability domains, however red curves (155 nM [Csk]) also have parts with one stable and two unstable states displaying excitable Src responses.

How are the period and amplitude of Src oscillations controlled by external cues? Signals, such as growth factor and cytokines, lead to dephosphorylation of the inhibitory phosphotyrosine pY_i, which is modeled as an increase in the RPTP activity, whereas an increase in the Csk activity raises the pY_i level (see the kinetic scheme in Fig. 1). Figs. 6A – 6D demonstrate significant frequency modulation by both activating and inhibitory stimuli and more moderate changes in the amplitude of the oscillations. An increase in the activating signal or decrease in the inhibitory signal decreases the period of Src oscillations. This frequency modulation resembles the previously described modulation of Ca^{2+} oscillations by increasing agonist concentration [44]. The

dependences of the period of oscillations on the RPTP and Csk concentrations almost mirror each other, although there are quantitative differences in the changes of the period within the oscillatory domain, a 2.7-fold decrease (from the highest to the lowest values) with a 1.5-fold RPTP increase and a 2.1-fold increase with a 1.7-fold Csk increase. Interestingly, the frequency modulation turns into opposite mode near one of the borders where the unstable steady state (shown by the dotted line) becomes stable, but the oscillations continue to persist within a small range after the Hopf bifurcation. The coexistence of oscillations (limit cycle) and a stable steady state implies subcritical Hopf bifurcation and the appearance of an unstable limit cycle. The unstable and stable limit cycles collide and annihilate in a global bifurcation near the oscillatory borders.

Saturability and consequent nonlinear rate dependencies do not change the repertoire of Src responses. A detailed analysis of the model shows that relaxing the simplifying assumption that steps 1, 2 and 5-7 follow linear, unsaturated kinetics (see Eq. 3) does not change the repertoire of Src dynamic responses discussed above. Moreover, saturability of step 4 (transition from the active S_{a1} to inactive S_i conformation) is critical for bistability and oscillations only when other steps follow linear kinetics, as was assumed initially for illustrative purposes. This condition can be replaced by saturability of step 5 or step 7 in the bypass from S_{a1} to S_i (Fig. 1). Fig. S4 (panels A, B) illustrates that both Src oscillatory patterns and bistability are observed when step 7 is saturable, whereas step 4 is not. However, since both steps 4 and 7 are catalyzed by the same enzyme (PTP1B), we also showed that all different types of the Src dynamics continue to occur when rates v_4 and v_7 are saturated by their substrates (Fig. S4 C, D).

Next, we examined how saturation of RPTP-catalyzed reactions 1 and 6 influences Src responses and found that all dynamic regimes described above still persist (Fig. S4 E, F). Interestingly, our calculations suggest that nonlinearities arising from saturability of steps catalyzed by PTP1B and Csk enlarge the bistability domain and decrease the oscillatory region in the parameter space, whereas saturability of RPTP-catalyzed steps exhibits the opposite effect. Likewise, the use of a more precise total QSS approximation [45, 46] that considers explicitly the concentrations of enzyme-enzyme complexes generated in autophosphorylation step 3 does not change our conclusions about diverse dynamics of the Src cycle. As illustrated in Fig. S5, which takes into account high concentrations of Src dimers, resulting in saturability of step 3, bistability, Src excitable switches, and oscillations can be observed for some degree of saturation.

Proposed experimental verification and conclusions.

Our findings of potentially bistable, oscillatory and excitable behavior of the Src cycle are awaiting experimental verification. The results based on the mathematical model suggest a feasible experimental design for *in vitro* tests of predictions about the Src dynamics. An advantage of an *in vitro* system with purified Src, Csk and relevant phosphatases is that it can be used to explore wide ranges of precisely set down enzyme concentrations. Although Src (de)activation reactions can proceed in solution [28, 31], the membrane localization of proteins will facilitate the formation of protein complexes and increase the reaction rates [35]. To mimic the *in vivo* situation, Src and other proteins can be embedded into a phospholipid membrane bilayer or liposomes. The Src cycle can be started by the addition of relevant phosphatases (or other Src activators, such as the SH2/SH3-ligands [38]) to activate step 1, followed by the addition of Csk and ATP to the reaction medium. At the selected time points aliquotes are taken, and the different phosphotyrosine levels that correspond to different Src conformations are measured by immunoblotting using specific antibodies (note that quantification of only the pY_a level is sufficient to obtain the kinetics of the active Src fractions). In addition, fluorescent resonance energy transfer (FRET) biosensors [47] can be exploited for high temporal resolution measurements of Src kinetics, e.g, oscillatory or excitable responses.

A pivotal condition for complex Src dynamics is intramolecular autophosphorylation that leads to a specific shape of the QSS dependence of the active Src fraction (s_1) on the inactive fraction (s_i), where a single s_1 value can correspond to three different s_i values (see Eq. 10 and Fig. 2). Therefore, we examined how this shape (generally referred to as a Z-shape) is affected by changes in each of the six kinetic parameters involved (Fig. S3). We found that when the ratio δ of the catalytic efficiencies of the partially and fully active forms (S and S_{a1}) is too large, the QSS curve of Eq. 10 becomes monotonic and loses its Z-shape (Fig. S3A). This phenomenon can be understood readily. Indeed, the important prerequisite for bistability is positive feedback [48], which is brought about by intermolecular phosphorylation of S by S_{a1} and S_{a2} in the Src cycle (Fig. 1). This autophosphorylation is equivalent to product activation that facilitates biological switches [34], whereas autophosphorylation of S catalyzed by the same form S counteracts this positive feedback and offsets bistable behavior. Likewise, small values of $k_4 = V_4^{\max} / S^{tot}$ will halt Src in a single high activity state (Fig. S3B). In addition, the loss of a Z-shape by the QSS curve and, therefore, the lack of complex dynamic regimes can result from increases in (*i*) $\beta = K_4 / S^{tot}$, (*ii*) the ratio ξ of quasi steady- state concentrations s_2 and s_1, and (*iii*) the rate constants k_3 and k_7 (Fig.

S3, C-F). This analysis of the parameter variation effects on the QSS curve is useful for experimental manipulations of the concentrations of both Src effectors and their competitive inhibitors (e.g., inactive mutants which lack catalytic activity, but bind Src), which will change the K_m values.

In an *in vitro* system the values of parameters, k_3, k_4 and β can be regulated by changing the Src abundance (S^{tot}). The analysis of regions with diverse Src dynamics in the plane of the Src abundance and k_1 demonstrates that both bistability and oscillatory regions exist above a threshold value of S^{tot} (Fig. 7). As shown in Fig. 7, changing the Src abundance and stimulus amplitude (k_1) ensues different Src dynamics, including monostable, bistable, oscillatory and excitable behavior.

We showed that Src biological switches and bistability might occur for both positive and negative slopes of the QSS curve determined by Eq. 11, whereas sustained oscillations and excitable Src behavior requires a positive slope. Thus, the sign of this slope is a critical parameter that determines the entire range of potential dynamics displayed by the Src cycle. The slope is positive, when Eq. 12 is satisfied, and inactive Src is regenerated preferentially from the double phosphorylated form of Src. In fact, this condition is supported by data [39, 40]. Instructively, the negative versus positive slope is implicated in a reverse relationship between inactive (s_i) and active (s_1, s_2) Src fractions during a switch-like transition from Off state to On state (in the bistability domain). Regardless of the slope, the active Src fractions increase during the Off to On transition, whereas the value of the inactive fraction (s_i) decreases if the slope is negative and increases otherwise (cf. Figs. 2A and 2B); a characteristic feature to be tested against the experiment.

Discussion

Src and other SFKs are known as proto-oncogenes, and altered Src activity is associated with human malignancies [3, 5]. Here we unveil novel, intrinsic features of the Src kinetic cycle and show that Src overexpression, increased stimulation by membrane receptors, or decreased inhibition do not merely hyperactivate Src, but can completely transform its temporal behavior and cellular responses. Our findings can help understand and explore deregulation of Src signaling in cancer. A central result of this work shows that all necessary prerequisites for the diverse, baroque dynamics of Src responses already exist in the absence of external feedback regulations. The Src (de)activation cycle alone can display bistable, oscillatory, and excitable behaviors, whereas

external effectors and complex regulatory loops are necessary to control potential Src responses in the cellular context.

The reaction topology of the Src kinetic cycle (Fig. 1) displays an illuminating structure, embracing two cycles of opposing (de)activation reactions and a "bypass" from an active conformation to an inactive conformation. We showed that biological switches (bistability), oscillations and excitable behavior are intrinsic to this kinetic structure. Even in the absence of bypass reactions (steps 5 – 7 in Fig. 1), intermolecular autophosphorylation (step 3) can bring about bistability and hysteresis (results not shown),which arise from implicit positive feedback that is equivalent to product activation [34]. Remarkably, intermolecular autophosphorylation is a recurrent topic in activation of a plethora of mammalian kinases [24-26], which warrants the exploration of the potential bistable behavior for many kinases. Interestingly, a reduced Src (de)activation cycle with only one active Src form (S_{a1}) can exhibit the complex dynamics. If for a moment we assume that steps 5 and 6 (Fig. 1) are much faster than the other steps in the Src cycle, the concentrations (s_2 and s_1) of two active Src forms become connected by the quasi-equilibrium relationship, $s_2 = K_{eq} s_1$, which formally coincides with Eq. 9 where $\xi = K_{eq}$. The reduced (planar) system with two independent variables (s_i and s_1) exhibits qualitatively the same complex dynamics that our original model (data not shown). We conclude that the presence of an additional, third independent variable is not absolutely essential for the complex dynamic behavior of Src.

In small membrane compartments where the number of SFK and effector molecules can be low, noise influences signaling dynamics. For instance, in the bistable regime where deterministic equations predict that Src activity is sustained at the high level or low level, depending on stimulus history, external or internal noise can lead to random switches between these two stable activity states. Interestingly, imposed positive feedback increases robustness to stochastic fluctuations and parameter variations. For example, although double phosphorylation in MAPK cascade can lead to bistability in the absence of any imposed positive feedback loops [21], positive feedback greatly enhances the robustness of the MAPK bistable switch to noise [49].

Our results can shed light on recent findings of propagating waves of Src activation along the plasma membrane [50]. In these experiments, human umbilical vein endothelial cells were mechanically stimulated by applying the laser-tweezer traction to fibronectin-coated beads adhering to the cells. As fibroneciton binds to integrins, the local pulling force stimulated integrins that subsequently activated Src. Intriguingly, the local Src activation triggered the long-range

propagation of active Src wave into the distal cell areas away from the site of mechanical stimulation [50]. The mechanism of this wave propagation is unknown and may include Src interactions with small GTPases and the cytoskeleton. Instructively, purely diffusive propagation of active Src is ruled out. In fact, in the absence of biochemical activation within the cell Src will be deactivated by inhibitory Csk phosphorylation already in the areas that are only at a small distance from the local stimuli [51]. Our findings suggest that Src traveling waves can be brought about by intrinsic bistable and/or excitable properties of the Src activation/deactivation cycle, just as trigger waves of kinase activity arise from bistability in kinase/phosphatase cascades [52].

Emerging evidence shows that SFKs are non-randomly distributed on the plasma and intracellular membranes, often localizing to specific microdomains with specialized functions, such as lipid rafts, caveolae, focal adhesions and other membrane microdomains [53]. Provided SFK molecules do not exchange rapidly between these microdomains, the bistable or oscillatory behavior will be manifested in each microdomain, converting an analog input signal into a defined digital signal. At the whole cell level this signal can become analog again. Thus, a cell can build a high-fidelity analogue–digital–analogue circuit to relay Src activity to downstream targets. Similarly, recently described Ras-GTP nanoswitches generate a high-fidelity analogue–digital–analogue circuit that transmits MAPK activation [54].

Importantly, phosphatases that regulate SFK activity are also distributed inhomogeneously. It was recently shown that there is a steady-state gradient of PTP1B activity across the cell with lower activity in the proximity of the plasma membrane and higher activity in the perinuclear area [36]. Such regulation of PTPB1 activity may generate distinct cellular environments for SFK signaling. For instance, in resting cells Src is localized in the perinuclear area, and when cells are stimulated with growth factors Src moves to the periphery [5, 55]. The plasma membrane recruitment and activation of Src kinase is required for focal adhesion. It is also thought to be essential for cellular transformation and is reported to be involved in the alignment of early endosomes along actin filaments [56]. These changes in Src localization that follow cell stimulation expose Src to different phosphatase activities, which may result in different dynamic behaviors in different cellular compartments.

We can usefully ask whether our findings can be applicable to other protein kinase families. Interestingly, the tetrameric subunit structure of the Abl/Arg and Tec kinase families (in particular, of the c-Abl kinase) resembles the SFK structures. The c-Abl kinase possesses three domains, SH2,

SH3, and the two-lobe kinase domain, which can group in a precisely similar manner as the corresponding SFK domains. For both c-Abl and SFK, the SH2-SH3 clamp prevents the two-lobe kinase domain to switch from a closed autoinhibited conformation to an open active conformation. Not surprisingly, it has long been thought that a Src-like switching mechanism might control the c-Abl kinase [30]. Furthermore, the diagrams of transitions between the different conformational states are similar for both kinases. Most importantly, the phosphorylation of tyrosine in the c-Abl activation loop, which is necessary for a transition into the fully active form is intramolecular autophosphorylation [25]. We suggest that the findings of the present paper are also applicable to the c-Abl kinase, which thus can exhibit the intricate dynamic behavior, the hypothesis awaiting the experimental verification.

Many SFKs initiate pathways required for DNA synthesis [57]. Complex signaling dynamics of SFK increases the repertoire of cellular responses to external cues. In fact, cell-fate decisions are often associated with the existence of two (or several) stable steady states. Bistability (or multistability) implies that under the same condition, the state of the cell can be very different, for instance, with high or low activity of kinases and expressions of particular genes. Instructively, excitable systems can also display two distinct kinds of outputs, exhibiting either low or high amplitude of responses to stimulus. Importantly, Src can show both bistable and excitable behavior, thus emerging as a robust manager of cell's fate.

Materials and methods

Software. Numerical integration, solving of implicit algebraic equations, and bifurcation analysis were performed using the Dbsolve software (http://www.biokinetics.ru) [58]. This software is based on numerical techniques, developed in [59]. The model SBML file is freely available and will be posted on the Journal website and author's website (http://cellnetworks.org).

Calculation of the QSS curves and steady states. The QSS curves were calculated using explicit expressions (see Eqs. 10, 11 and the legend to Fig. S1). The dependencies of steady states on parameters were calculated by continuation techniques described in [59] and implemented in Dbsolve [58].

Determination of bifurcation boundaries. Numerical algorithms that are implemented in Dbsolve use a continuation approach and find local bifurcations as follows [59]. The saddle-node bifurcation curve is found by equating the determinant of the Jacobian matrix of Eqs 6-8 to zero (fold bifurcation). The Hopf bifurcation curve is determined by equating the sum of the two

eigenvalues to zero and taking only those parts of the curve where both eigenvalues are purely imaginary.

Acknowledgments

We thank Dr. W. Kolch for discussions and critical reading of the manuscript. This work was supported by the NIH grants GM059570 and R33HL088283.

References

1. Parsons SJ & Parsons JT (2004) Src family kinases, key regulators of signal transduction. *Oncogene* **23**, 7906-7909.
2. Roskoski R, Jr. (2005) Src kinase regulation by phosphorylation and dephosphorylation. *Biochem Biophys Res Commun* **331**, 1-14.
3. Frame MC (2002) Src in cancer: deregulation and consequences for cell behaviour. *Biochim Biophys Acta* **1602**, 114-130.
4. Martin GS (2001) The hunting of the Src. *Nat Rev Mol Cell Biol* **2**, 467-475.
5. Yeatman TJ (2004) A renaissance for SRC. *Nat Rev Cancer* **4**, 470-480.
6. Donella-Deana A, Cesaro L, Ruzzene M, Brunati AM, Marin O & Pinna LA (1998) Spontaneous autophosphorylation of Lyn tyrosine kinase at both its activation segment and C-terminal tail confers altered substrate specificity. *Biochemistry* **37**, 1438-1446.
7. Sun G, Sharma AK & Budde RJ (1998) Autophosphorylation of Src and Yes blocks their inactivation by Csk phosphorylation. *Oncogene* **17**, 1587-1595.
8. Boerner RJ, Kassel DB, Barker SC, Ellis B, DeLacy P & Knight WB (1996) Correlation of the phosphorylation states of pp60c-src with tyrosine kinase activity: the intramolecular pY530-SH2 complex retains significant activity if Y419 is phosphorylated. *Biochemistry* **35**, 9519-9525.
9. Chappel J, Ross FP, Abu-Amer Y, Shaw A & Teitelbaum SL (1997) 1,25-dihydroxyvitamin D3 regulates pp60c-src activity and expression of a pp60c-src activating phosphatase. *J Cell Biochem* **67**, 432-438.
10. Gil-Henn H & Elson A (2003) Tyrosine phosphatase-epsilon activates Src and supports the transformed phenotype of Neu-induced mammary tumor cells. *J Biol Chem* **278**, 15579-15586.
11. Granot-Attas S & Elson A (2004) Protein tyrosine phosphatase epsilon activates Yes and Fyn in Neu-induced mammary tumor cells. *Exp Cell Res* **294**, 236-243.
12. Zheng XM, Resnick RJ & Shalloway D (2000) A phosphotyrosine displacement mechanism for activation of Src by PTPalpha. *Embo J* **19**, 964-978.
13. Brown MT & Cooper JA (1996) Regulation, substrates and functions of src. *Biochim Biophys Acta* **1287**, 121-149.
14. Simons K & Toomre D (2000) Lipid rafts and signal transduction. *Nat Rev Mol Cell Biol* **1**, 31-39.
15. Thomas SM & Brugge JS (1997) Cellular functions regulated by Src family kinases. *Annu Rev Cell Dev Biol* **13**, 513-609.
16. Roche S, Fumagalli S & Courtneidge SA (1995) Requirement for Src family protein tyrosine kinases in G2 for fibroblast cell division. *Science* **269**, 1567-1569.
17. Fuss H, Dubitzky W, Downes S & Kurth MJ (2006) Bistable switching and excitable behaviour in the activation of Src at mitosis. *Bioinformatics* **22**, e158-165.
18. Fuss H, Dubitzky W, Downes CS & Kurth MJ (2007) Deactivation of Src family kinases: hypothesis testing using a Monte Carlo sensitivity analysis of systems-level properties. *J Comput Biol* **14**, 1185-1200.
19. Fuss H, Dubitzky W, Downes CS & Kurth MJ (2008) SRC family kinases and receptors: analysis of three activation mechanisms by dynamic systems modeling. *Biophys J* **94**, 1995-2006.
20. Ferrell JE, Jr. (2002) Self-perpetuating states in signal transduction: positive feedback, double-negative feedback and bistability. *Curr Opin Cell Biol* **14**, 140-148.
21. Markevich NI, Hoek JB & Kholodenko BN (2004) Signaling switches and bistability arising from multisite phosphorylation in protein kinase cascades. *J Cell Biol* **164**, 353-359.

22. Novak B, Tyson JJ, Gyorffy B & Csikasz-Nagy A (2007) Irreversible cell-cycle transitions are due to systems-level feedback. *Nat Cell Biol* **9**, 724-728.
23. Qiao L, Nachbar RB, Kevrekidis IG & Shvartsman SY (2007) Bistability and oscillations in the Huang-Ferrell model of MAPK signaling. *PLoS Comput Biol* **3**, 1819-1826.
24. Rogers JA, Read RD, Li J, Peters KL & Smithgall TE (1996) Autophosphorylation of the Fes tyrosine kinase. Evidence for an intermolecular mechanism involving two kinase domain tyrosine residues. *J Biol Chem* **271**, 17519-17525.
25. Brasher BB & Van Etten RA (2000) c-Abl has high intrinsic tyrosine kinase activity that is stimulated by mutation of the Src homology 3 domain and by autophosphorylation at two distinct regulatory tyrosines. *J Biol Chem* **275**, 35631-35637.
26. Donella-Deana A, Cesaro L, Sarno S, Brunati AM, Ruzzene M & Pinna LA (2001) Autocatalytic tyrosine-phosphorylation of protein kinase CK2 alpha and alpha' subunits: implication of Tyr182. *Biochem J* **357**, 563-567.
27. Caron-Lormier G & Berry H (2005) Amplification and oscillations in the FAK/Src kinase system during integrin signaling. *J Theor Biol* **232**, 235-248.
28. Barker SC, Kassel DB, Weigl D, Huang X, Luther MA & Knight WB (1995) Characterization of pp60c-src tyrosine kinase activities using a continuous assay: autoactivation of the enzyme is an intermolecular autophosphorylation process. *Biochemistry* **34**, 14843-14851.
29. Young MA, Gonfloni S, Superti-Furga G, Roux B & Kuriyan J (2001) Dynamic coupling between the SH2 and SH3 domains of c-Src and Hck underlies their inactivation by C-terminal tyrosine phosphorylation. *Cell* **105**, 115-126.
30. Harrison SC (2003) Variation on an Src-like theme. *Cell* **112**, 737-740.
31. Sun G, Ramdas L, Wang W, Vinci J, McMurray J & Budde RJ (2002) Effect of autophosphorylation on the catalytic and regulatory properties of protein tyrosine kinase Src. *Arch Biochem Biophys* **397**, 11-17.
32. Smith JA, Francis SH & Corbin JD (1993) Autophosphorylation: a salient feature of protein kinases. *Mol Cell Biochem* **127-128**, 51-70.
33. Hardwick JS & Sefton BM (1997) The activated form of the Lck tyrosine protein kinase in cells exposed to hydrogen peroxide is phosphorylated at both Tyr-394 and Tyr-505. *J Biol Chem* **272**, 25429-25432.
34. Kholodenko BN (2006) Cell-signalling dynamics in time and space. *Nat Rev Mol Cell Biol* **7**, 165-176.
35. Kholodenko BN, Hoek JB & Westerhoff HV (2000) Why cytoplasmic signalling proteins should be recruited to cell membranes. *Trends Cell Biol* **10**, 173-178.
36. Yudushkin IA, Schleifenbaum A, Kinkhabwala A, Neel BG, Schultz C & Bastiaens PI (2007) Live-cell imaging of enzyme-substrate interaction reveals spatial regulation of PTP1B. *Science* **315**, 115-119.
37. Bromann PA, Korkaya H & Courtneidge SA (2004) The interplay between Src family kinases and receptor tyrosine kinases. *Oncogene* **23**, 7957-7968.
38. Yadav SS & Miller WT (2007) Cooperative activation of Src family kinases by SH3 and SH2 ligands. *Cancer Lett* **257**, 116-123.
39. Bougeret C, Delaunay T, Romero F, Jullien P, Sabe H, Hanafusa H, Benarous R & Fischer S (1996) Detection of a physical and functional interaction between Csk and Lck which involves the SH2 domain of Csk and is mediated by autophosphorylation of Lck on tyrosine 394. *J Biol Chem* **271**, 7465-7472.

40. Amrein KE, Molnos J, zur Hausen JD, Flint N, Takacs B & Burn P (1998) Csk-mediated phosphorylation of substrates is regulated by substrate tyrosine phosphorylation. *Farmaco* **53**, 266-272.
41. Laird AD & Shalloway D (1997) Oncoprotein signalling and mitosis. *Cell Signal* **9**, 249-255.
42. Kholodenko BN (2007) Untangling the signalling wires. *Nat Cell Biol* **9**, 247-249.
43. Kholodenko BN (2000) Negative feedback and ultrasensitivity can bring about oscillations in the mitogen-activated protein kinase cascades. *Eur J Biochem* **267**, 1583-1588.
44. Rooney TA, Sass EJ & Thomas AP (1989) Characterization of cytosolic calcium oscillations induced by phenylephrine and vasopressin in single fura-2-loaded hepatocytes. *J Biol Chem* **264**, 17131-17141.
45. Borghans JA, de Boer RJ & Segel LA (1996) Extending the quasi-steady state approximation by changing variables. *Bull Math Biol* **58**, 43-63.
46. Tzafriri AR & Edelman ER (2004) The total quasi-steady-state approximation is valid for reversible enzyme kinetics. *J Theor Biol* **226**, 303-313.
47. Ouyang M, Sun J, Chien S & Wang Y (2008) Determination of hierarchical relationship of Src and Rac at subcellular locations with FRET biosensors. *Proc Natl Acad Sci U S A* **105**, 14353-14358.
48. Thomas R, Gathoye AM & Lambert L (1976) A complex control circuit. Regulation of immunity in temperate bacteriophages. *Eur J Biochem* **71**, 211-227.
49. Smolen P, Baxter DA & Byrne JH (2008) Bistable MAP kinase activity: a plausible mechanism contributing to maintenance of late long-term potentiation. *Am J Physiol Cell Physiol* **294**, C503-515.
50. Wang Y, Botvinick EL, Zhao Y, Berns MW, Usami S, Tsien RY & Chien S (2005) Visualizing the mechanical activation of Src. *Nature* **434**, 1040-1045.
51. Kholodenko BN (2003) Four-dimensional organization of protein kinase signaling cascades: the roles of diffusion, endocytosis and molecular motors. *J Exp Biol* **206**, 2073-2082.
52. Markevich NI, Tsyganov MA, Hoek JB & Kholodenko BN (2006) Long-range signaling by phosphoprotein waves arising from bistability in protein kinase cascades. *Mol Syst Biol* **2**, 61.
53. de Diesbach P, Medts T, Carpentier S, D'Auria L, Van Der Smissen P, Platek A, Mettlen M, Caplanusi A, van den Hove MF, Tyteca D, et al. (2008) Differential subcellular membrane recruitment of Src may specify its downstream signalling. *Exp Cell Res* **314**, 1465-1479.
54. Tian T, Harding A, Inder K, Plowman S, Parton RG & Hancock JF (2007) Plasma membrane nanoswitches generate high-fidelity Ras signal transduction. *Nat Cell Biol* **9**, 905-914.
55. Sandilands E, Brunton VG & Frame MC (2007) The membrane targeting and spatial activation of Src, Yes and Fyn is influenced by palmitoylation and distinct RhoB/RhoD endosome requirements. *J Cell Sci* **120**, 2555-2564.
56. Gasman S, Kalaidzidis Y & Zerial M (2003) RhoD regulates endosome dynamics through Diaphanous-related Formin and Src tyrosine kinase. *Nat Cell Biol* **5**, 195-204.
57. Choudhury GG, Mahimainathan L, Das F, Venkatesan B & Ghosh-Choudhury N (2006) c-Src couples PI 3 kinase/Akt and MAPK signaling to PDGF-induced DNA synthesis in mesangial cells. *Cell Signal* **18**, 1854-1864.
58. Goryanin I, Hodgman TC & Selkov E (1999) Mathematical simulation and analysis of cellular metabolism and regulation. *Bioinformatics* **15**, 749-758.
59. Khibnik AI, Kuznetsov YA, Levitin VV & Nikolaev EV (1993) Continuation techniques and interactive software for bifurcation analysis of ODEs and iterated maps. *Physica D* **62**, 360-371.

Supplementary material

The following supplementary material is available online:

Table S1. Ranges of kinetic parameters.

Fig. S1. Graphical and analytical solutions of the QSS equations for the kinetic model.

Fig. S2. Proximity of Src initial state to the excitability threshold decreases the lag period.

Fig. S3. Complete numerical investigation of the dependence of the Z-shaped QSS curve on each kinetic parameter involved.

Fig. S4. Effects of saturabilities of reaction rates on the QSS dependencies.

Fig. S5. Effects of large concentrations of Src dimers on the QSS dependence.

Figure legends

Fig. 1. Kinetic scheme of the Src activation/deactivation cycle. Four possible forms of the Src molecule are shown. S_i is the autoinhibited conformation where the inhibitory tyrosine residue is phosphorylated and the activatory residue is dephosphorylated, S is the partially active form where both the inhibitory and activatory residues are dephosphorylated, S_{a1} is the fully active conformation where the inhibitory tyrosine residue is dephosphorylated and the activatory residue is phosphorylated, and S_{a2} is the fully active form where both the inhibitory and activatory residues are phosphorylated. The solid lines with arrows present the Src cycle reactions catalyzed by the indicated enzymes. The dotted green lines specify intermolecular autophosphorylation reactions.

Fig. 2. Different types of QSS curve intersections determine the Src cycle steady states and dynamics. One stable steady state (O) or three steady states (stable O_1 and O_3 and unstable O_2) exist for both positive (panels **A, C**) and negative (**B**) slopes of the linear (blue) QSS curve (Eq.11), which intersects the Z-shaped (black) QSS curve (Eq.10). The parameter values are (**A**) k_1=0.2 s^{-1} (line 1), 0.34 s^{-1} (2) and 0.6 s^{-1} (3), k_2=0.3 s^{-1}. (**B**) k_1=0.5 (1), 0.8 (2) and 1.5 (3), k_2=1 (all rate constants are in s^{-1}). **C.** A single unstable steady state (O) surrounded by a limit cycle (red), which corresponds to stable oscillatory pattern of Src activity, k_1=0.1, k_2=0.01, k_5=2, k_6=1 (s^{-1}). The resting state *in vivo* ($s_i = 0.916$, $s_1 = s_2 = 7.32 \cdot 10^{-5}$) was taken as the initial condition ("rest"), the movement direction is shown by arrows. For all curves in **A – C** the remaining parameters are, k_3=20, k_4=1, k_7=1 (s^{-1}), β=0.01, δ=0.05, ξ=1.

Fig. 3. Bistability and oscillations in the Src cycle. A. Hysteresis in steady-state responses of active Src fraction (s_1) to changes in the active RPTP concentration ([RPTP]). Dotted line corresponds to unstable steady states located at the intermediate branch of the curve between turning points P_1 and P_2 (marked bold). **B.** The time dependence of s_1 responses to stepwise changes in active [RPTP]; these changes are conditionally taken as 9 nM variations. Arrows in **B** show the time point of step changes in [RPTP]. The corresponding [RPTP] values, 117.5, 126.5 and 135.5 (nM), are indicated by dashed lines 1 - 3 in **A** and shown by upper line in **B**. The catalytic efficiency of RPTP (steps 1 and 6) is $k^{cat}/K_M = 3.6 \cdot 10^{-3}$ and 0.02 ($nM^{-1}s^{-1}$); the first-order rate constants, k_1 and k_6 are calculated as k^{cat}[RPTP]/K_M (Eq. 3); k_2=0.5, k_5=10 (s^{-1}). **C.** Sustained oscillations of Src fractions (s_1 – black, s_2 – red, s_i – black, s - blue). The time behavior corresponds to the limit cycle trajectory shown in Fig. 2C, arrows indicate the onset of stimulation,

k_1 = 0.1; k_2=0.01, k_5=2, k_6=1 (s^{-1}). For all curves in **A - C**, the remaining parameters are given in the legend to Fig. 2.

Fig. 4. Src excitable behavior in response to rectangular pulse inputs (A, B) and perturbations to the initial concentrations (C, D). Initially Src resides in a stable, but excitable steady state. For sub-threshold or over threshold stimuli, responses of the active Src fractions, s_1 and s_2, remain small or undergo large excursions generating high-amplitude responses, before returning to the same basal steady state. **A.** At time t_0 = 5 s (marked by arrow), the rate constant k_1 was increased from the basal level of 0.001 to 0.1 s^{-1} (from point 1 on panel **B** to the level that corresponds to the unstable steady state, point 2). After time $t_1 = t_0 + 9$ s (bold line 1) or $t_2 = t_0 +$ 10 s (bold line 2), k_1 was decreased to the basal level. The time-dependent responses of the active Src fractions, s_1 (black) and s_2 (blue) are shown by dashed and solid lines for 9 and 10 s stimulation periods, respectively. **B.** The trajectories (red) that correspond to the time-dependent responses in A and the QSS curves (black and blue) are shown in the plane of s_1 and s_2. **C.** At time t_0 = 5 s, a perturbation (Δs_1) to the steady state increased s_1 from 0.0082 to 0.03 (point 1) or 0.04 (point 2). Accordingly, the following equation was used for the total of the normalized concentrations, $s_i + s + s_1 + s_2 = 1 + \Delta s_1$. The time-dependent responses to a sub-threshold perturbation (starting from point 1) and to a perturbation over threshold (starting from point 2) are shown by dashed and solid lines, respectively. **D.** The trajectories (red) that correspond to the time-dependent responses in C and the QSS curves (black and blue) are shown in the plane of s_i and s_1. k_1=0.03 s^{-1}. For all plots shown in **A - D,** the remaining parameters are given in the legend to Fig. 2C.

Fig. 5. Bifurcation diagrams unveil different Src dynamics. A. In the plane of active RPTP and Csk concentrations, bifurcation boundaries separate regions of different types of Src dynamics, determined by the Hopf (red lines) and saddle-node (black lines) bifurcations. These regions are numbered as follows, 1 – a single stable steady state, 2 – bistability domain, two stable states separated by a saddle, 3 – oscillations, a single unstable steady state, 4 – oscillations, three unstable steady states, 5 – one stable and two unstable steady states. Dashed line parallel to the [RPTP] axis crosses the plane at 25 nM [Csk]. Insert shows the zoomed-in region 4. **B.** One parameter bifurcation diagrams represent steady-state dependencies of Src active and inactive fractions s_1 and s_i on [RPTP] at four different constant [Csk] values, indicated near each curve (curves have different colors). Closed circles are turning points; dotted lines correspond to

unstable steady states. Csk catalytic efficiency is, k^{cat}/K_M = 0.002 and 0.04 ($nM^{-1}s^{-1}$) for steps 2 and 5; the first-order rate constants, k_2 and k_5 are calculated as k^{cat}[Csk]/K_M (Eq. 3). The remaining parameters are the same as in the legend to Fig. 3.

Fig 6. Control of the period and amplitude of Src oscillations by the activities of the activatory phosphatase RPTP and inhibitory kinase Csk. Dependence of the oscillation amplitude (**A**) and period (**B**) on the active RPTP concentration at constant Csk concentration (25 nM). The amplitude is the difference between maximal (s_{1max}) and minimal (s_{1min}) values of the relative active Src fraction (red curves). Black solid line indicates stable steady states, whereas the dotted black line shows unstable steady states (steady state values are designated as s_{1SS}). Dependence of the oscillation amplitude (**C**) and period (**D**) on the active Csk concentration at constant RPTP concentration (30 nM). The parameter values are indicated in the legend to Fig. 5.

Fig. 7. Bifurcation diagram in the plane of the rate constant k_1 and total Src abundance. k_1 is the rate constant of dephosphorylation of inhibitory tyrosine in the Src C-terminus. Types of bifurcation boundaries and the numbering of regions with different Src dynamics are the same as in Fig. 5. Src autocatalytic efficiency is k_{a1}^{cat}/K_{a1} =0.05 $nM^{-1}s^{-1}$, V_4^{max} =400 nM/s, K_4=4 nM. The remaining parameters are the same as in the legend to Fig. 3. Insert shows the zoomed-in region 4.